The final publication is available at Elsevier via https://dx.doi.org/10.1016/j.ijfatigue.2018.03.019 © 2019. This manuscript version is made available under the CC-BY-NC-ND 4.0 license https://creativecommons.org/licenses/by-nc-nd/4.0/

Accepted Manuscript

Fatigue Characteristics and modeling of Cast and Cast-Forged ZK60 Magnesium Alloy

S.M.H. Karparvarfard, S.K.Shaha, S.B. Behravesh, H. Jahed, B.W. Williams

PII: S0142-1123(18)30111-7
DOI: https://doi.org/10.1016/j.ijfatigue.2018.03.019
Reference: JIJF 4620

To appear in: *International Journal of Fatigue*

Received Date: 16 November 2017
Revised Date: 13 March 2018
Accepted Date: 17 March 2018

Please cite this article as: Karparvarfard, S.M.H., S.K.Shaha, Behravesh, S.B., Jahed, H., Williams, B.W., Fatigue Characteristics and modeling of Cast and Cast-Forged ZK60 Magnesium Alloy, *International Journal of Fatigue* (2018), doi: https://doi.org/10.1016/j.ijfatigue.2018.03.019

This is a PDF file of an unedited manuscript that has been accepted for publication. As a service to our customers we are providing this early version of the manuscript. The manuscript will undergo copyediting, typesetting, and review of the resulting proof before it is published in its final form. Please note that during the production process errors may be discovered which could affect the content, and all legal disclaimers that apply to the journal pertain.

ACCEPTED MANUSCRIPT

Fatigue Characteristics and modeling of Cast and Cast-Forged ZK60 Magnesium Alloy

S.M.H. Karparvarfard[1], S.K.Shaha[1], S.B. Behravesh[1], H. Jahed[1*], B.W. Williams[2]

[1]Department of Mechanical & Mechatronics Engineering, University of Waterloo, 200 University Ave W, Waterloo, ON, N2L 3G1, CANADA

[2]CanmetMATERIALS, Natural Resources Canada, 183 Longwood Road South, Hamilton, ON, L8P 0A1, Canada

Corresponding author's email address: hamid.jahed@uwaterloo.ca

Abstract

The fatigue behavior of as-cast and cast-forged ZK60 magnesium alloy was investigated via fully-reversed strain controlled fatigue tests at different strain amplitudes. Microstructure analysis, texture measurement, and SEM fracture surface characterization were performed to discern the reason of fatigue behavior improvement via forging, and also to explain the mechanism underlying crack initiation in both cast and cast-forged conditions. It was perceived that the forged alloy contains less amount of porosities and second phase particles in its microstructure. In general, the forged alloy showed longer fatigue life for all strain amplitudes, especially when the strain amplitude is lower than 0.4%. The forging process increased the fatigue strength at 10^7 cycles from 0.175% to 0.22% strain amplitude. The microstructure obtained after fatigue test showed that twinning can be activated in the cast-forged alloy, once strain amplitude is higher than 0.4%. The interaction of twin bands with the grain boundaries can also adversely affect the fatigue life of the forged alloy. Also, the residual twins can develop tensile mean stress which affects the fatigue life negatively. Finally, the Coffin-Manson fatigue model and an energy-based fatigue model were employed to model the life of as-cast and cast-forged materials. While some of the predicted lives by the former were out of the ±2x boundary bounds, the latter's results were tightly clustered in ±1.5x bounds.

Keywords: Magnesium alloys; Forging; As-cast alloys; Fatigue behavior; Life modeling.

ACCEPTED MANUSCRIPT

1. Introduction

Since the 1920s, steel has been an integral material utilized in cars [1]. However, environmental concerns have driven new interests for cutting down on the vehicles' mass. It was reported that 10% reduction of the vehicles' weight would lead to the saving of the cars' fuel consumption rates of approximately 5% [2]. Therefore, magnesium (Mg), which is the lightest commercially available metal, has attracted the interest of the automotive industry [3]–[6].

Magnesium has a hexagonal closed-pack (HCP) crystallographic microstructure which brings about limited deformability at ambient temperature. According to the Taylor criterion, five independent deformation modes are needed to accommodate strains during a deformation for a polycrystalline material [7]; however, the HCP crystal structure provides Mg with a limited number of deformation modes which are active at low temperatures. Thus, twins are activated for homogeneous deformation which form strong basal texture and reduce the deformability at room temperature[8][9]. On the contrary, this mode of deformation cannot be activated along all the loading directions [10][11]. Workability will be improved at higher temperatures, as additional slip systems are sufficiently activated [12][13].

Die-casting is the most prevalent method of manufacturing of Mg parts for its economic advantages [14]. Nonetheless, it leaves casting defects such as porosities and inclusions in the microstructure which are deleterious to the material's mechanical behavior [15]. Therefore, for structural applications, where high strength and workability are required, wrought Mg alloys are preferred over cast Mg alloys [6]. Wrought alloys have shown superior fatigue response and higher strength and ductility as a result of grain refinement and containing lower amount of defects with second phase particles [16][17][18][19][20].

Currently, the application of Mg alloys in the automotive industry is limited to non-load bearing components such as instrument panel, seat frame, and housing parts [6]. However, to accomplish the target of mass reduction, expanding its applications to the load-bearing components is indispensable. Accordingly, studying the mechanical behavior of wrought Mg alloys, and in particular, the fatigue behavior, has been the topic of a number of studies in the last decade. Main attention has been devoted to AZ-series of Mg alloys as compared to ZK-series. ZK- series Mg alloys have shown high strength and formability due to the presence of Zr as grain refiner [21][22][23]. Liu et al. [24] investigated the tensile and high cycle fatigue (HCF)

ACCEPTED MANUSCRIPT

behavior of extruded and T5 heat treated ZK60 under load-controlled fatigue. They reported that the T5 heat treatment refined the grain structure from bimodal to more equiaxed grains with higher pole figure intensity of fiber texture which basically improved the performance of ZK60; especially the fatigue strength improved from 140 to 150 MPa. Other studies [25][26][27] investigated the cyclic behavior of the extruded ZK60 along the extrusion direction through fully-reversed stress and strain controlled cyclic tests to understand the twining/detwinning activity. They revealed that the activation of twinning and detwinning during the cyclic loading increased with increasing the strain amplitude beyond 4% due to the asymmetric behavior in tension-compression, while the slip was dominated at lower stress/strain amplitude.

Several manufacturing processes have been employed to achieve grain refinement through forming of Mg alloys [19][28][29] [30][31]. Among a wide variety of processing methods, forging is of particular interest because it has shown its promise to produce components with complex geometries [32][33][34]. However, only a few studies have been performed to isolate the contribution of the forging process to the cyclic behavior of Mg alloys. Vasilev et al. [35] carried out a study on the effects of multiaxial isothermal forging (MIF) on the microstructure and fatigue behavior of as-cast ZK60. The results demonstrated that nearly 80% of coarse grains volume fraction was refined after MIF, which causes better fatigue response in both LCF and HCF regimes. However, limited number of studies has been contributed to the effects of forging process on the as-cast Mg alloys in particular as-cast ZK60. Recently, Gryguc et al. [36], [37] and Toscano et al. [38] studied the influence of forging on the mechanical properties, and in particular cyclic response, of AZ80 and AZ31B Mg alloys, respectively. They revealed that a significant grain refinement was achieved in forged components, which improved the fatigue life of the cast or extruded Mg alloy. In another study, the authors have characterized the quasi static tensile and compressive behavior of cast-forged ZK60 [39] and showed ZK60's great potentials to be utilized in load-bearing components of vehicles. However, the fatigue behavior of the forged ZK60 alloy has not yet been comprehensively investigated. In this paper we investigate the fatigue behavior of cast and cast-forged ZK60. Toward this objective, strain controlled fully reversed push-pull fatigue tests have been performed. Texture and microstructural analysis, and SEM fracture surface analysis were carried out to discern the mechanical behavior, and to identify the mechanism underlying crack initiation and failure. Moreover, two common fatigue models were utilized to discuss the obtained fatigue results.

ACCEPTED MANUSCRIPT

2. Material and Methods

The starting material in the present study was an as-cast ZK60 ingot with the dimensions of 300 mm diameter and 500 mm length. The chemical composition of the alloy is presented in [39]. The ingot was then machined into cylinders with a diameter of 63.5 mm and a length of 65 mm, which were used as forging billets. Each billet was heated at the temperature of 450°C for 3.5 hours, and transferred to the forging anvil, which was also heated up to the same temperature. The open-die forging process was then performed at the ram speed of 390 mm/min along the radial direction, as shown schematically in Figure 1. As discussed in our previous study [39], the temperature of 450°C was selected for the forging, as it is above the lowest melting temperature of the eutectic phase for ZK60, 339.5°C [40]. It is therefore expected that the second phase particles were dissolved into the matrix, which could lead to a better forging response. Also, Hadadzadeh et al. [41] investigated the same material exploiting a Gleeble® 3500 thermal-mechanical simulation testing system, and observed no incipient melting in the microstructure at 450°C. Regarding the ram speed of 390 mm/min, it should be stated that forging trials had been performed at four different speeds of 0.39 mm/min, 3.9 mm/min, 39 mm/min, and 390 mm/min [42]. It was observed that the mechanical behavior of the materials under compression loading is the same. Hence, for practical purposes, and to save the time and energy, the highest ram speed was chosen for investigation in this study.

Microstructures and texture analysis were carried out on samples collected from both as-cast and forged conditions. The samples were initially ground with SiC sand papers, and later polished with 6, 3, 1, and 0.1 micron diamond pastes. After that, polishing was performed using colloidal silica. Finally, the samples were etched utilizing an acetic-picral etchant. Texture measurement was done with a Bruker D8 Discover X-ray diffractometer equipped with an advanced 2D-detector using CuKα beam radiation at the voltage of 40 kV and current of 40 mA. The obtained diffraction patterns were evaluated using Bruker trademark software DIFFRAC.EVA. Further details about the texture analysis are explained in [43].

Smooth dog-bone samples were machined from the as-cast and forged ZK60 materials. The specimen locations and corresponding labelling are shown in Figure 2(a) and (b) for the as-cast and forged ZK60, respectively. The as-cast specimens were cut along two different

ACCEPTED MANUSCRIPT

directions, i.e., radial (RD) and longitudinal (LD) directions. To avoid inconsistency, all the samples from the as-cast billet were cut at the distance of the 75% of the billet radius. However, the specimens from the forged material were cut along only one direction, i.e., LD. The FD in Figure 2(b) represents the forging direction. The specimen geometry can be found in [39].

Fatigue tests were performed under standard laboratory condition, as per ASTM E606/E606M-12 standard, using an Instron 8874 servo-hydraulic frame having a load capacity of ±25 kN. Engineering strain values were measured during the tests using a uniaxial epsilon extensometer with a gauge length of 8 mm and travel distance of ±0.8 mm. All the experiments were conducted under fully revered (R = -1) strain controlled condition. The loading frequency was selected between 0.2 and 1 Hz to achieve the same strain rate of 10^{-2} sec^{-1} throughout the fatigue tests. At very low strain amplitudes and after the material's behavior was stabilized, the tests were shifted to load controlled mode at a higher frequency of up to 30 Hz and continued up to 10^7 cycles. Tests with no failure at 10^7 cycles were stopped and considered as run-out tests. Fatigue life was assumed to be the life at rupture. Each test was at least once duplicated to verify the reproducibility of the results. The number of test specimens and percent replication was based on ASTM E739-10 standard. Finally, fracture surfaces were analyzed under SEM to describe the mechanism underlying the crack initiation, propagation, and final failure.

3. Results and Discussion

3.1. Texture and Microstructure

Figure 3(a) and (b) depict the microstructure of the as-cast ZK60 in the un-etched and etched conditions, respectively. As seen, the microstructure of ZK60 cast is laden with dendrites and porosities. A secondary dendritic arm spacing (SDAS) of 35±6 µm and a grain size of 104 ±25 µm was observed in the as-cast material. The presence of Zn- and Zr- rich intermetallics ($MgZn_2$ and Zn_2Zr) in the microstructure has already been reported in the literature, detected using EDX line scanning and XRD analysis [39][40]. For the forged material, however, as shown in Figure 3(c) and (d), grains were finer with the average size of 2–5 µm, and the porosity fraction was reduced significantly. Moreover, the volume fraction of second phase particles was reduced in the microstructure of forged alloy in comparison to the as-cast alloy, since during the forging

ACCEPTED MANUSCRIPT

process some intermetallics dissolve back into the matrix. While 15% volume fraction of the microstructure of as-cast ZK60 contained porosities and second phase particles, that amount was promisingly reduced to 5% for the forged alloy. This can lead to better fatigue response, as intermetallic particles are notable sites for crack initiation due to stress concentration [44]. Porosities can also play a major role in premature failure. These vacancies can coalesce and make a void leading to a crack that can cause the final fracture [45]. In addition, dendrites can accommodate pores and play as walls between the grains, and decreasing the SDAS results in superior strength of the material [46].

Figure 4 shows the texture measurement results for the as-cast and forged materials. While the as-cast alloy shows a random texture, where grains are not orientated mainly along any specific direction, a strong basal texture can be observed in the forged alloy. Specifically, the pole figures (PF) for the basal (0002) and prismatic $(10\bar{1}0)$ planes indicated a maximum intensity of 5.7 and 2.21, respectively; thereby, the HCP unit cell of the forged alloy are primarily aligned such that the c-axis is parallel to the forging direction.

3.2. Quasi-static uniaxial tensile behavior

A comprehensive investigation of the quasi-static uniaxial behavior of the as-cast and forged ZK60 alloys has already been delivered in the previous study by the authors [39]. Table 1 shows the tensile properties of the as-cast and forged alloy under uniaxial tensile loading along LD direction. As reported in [39], the quasi-static uniaxial behavior of ZK60 is similar in both, LD and RD directions at both as-cast and forged conditions.

3.3. Cyclic behavior

Fatigue tests were performed under strain control mode at different strain amplitudes ranging from 0.15% to 0.9%. Detailed summary of uniaxial cyclic tests is presented in Table 2 which includes the applied strain amplitudes (elastic and plastic strain amplitudes), the total life, the maximum and minimum stresses, and the elastic and plastic strain energy densities for the half-life cycles. Figure 5 depicts the typical engineering stress-strain hysteresis loops for the second and half-life cycles at the total strain amplitudes of 0.3%, 0.5%, and 0.7% for the as-cast and cast-forged conditions. It is noticed that the cyclic behavior of as-cast ZK60 is symmetric during the whole cyclic life at different strain amplitudes (Figure 5(a), (b), and (c)), 3 distinct types of

ACCEPTED MANUSCRIPT

behavior can be inferred for the forged alloy. They are (i) symmetric (ii) partially symmetric and (ii) asymmetric behavior in hysteresis loops. Firstly, for the strain amplitudes lower than 0.4%, Figure 5(d), the forged alloy exhibits symmetric hysteresis loop in the second cycle, whereas no plateau in the compression reversal can be seen, which signifies that the twinning is not activated [11][47][48]. Moreover, while marginal strain hardening is occurring during the history of cyclic loading, as the tensile peak stress is increased in the half-life hysteresis, still no sign of twinning is present in the compression reversal. At higher strain amplitude of 0.5%, Figure 5(e), it is seen that twinning is driving the deformation under compression loading after the strain of ~ -0.3%, and detwining is active till about the strain of 0.03% in the second cycle. In contrast, the half-life hysteresis loop indicates that the strain is primarily accommodated by the slip mode of deformation, since no zero-work hardening plateau can be seen under compressive loading. It is believed that this remarkable change in the hysteresis loop shape is owing to the exhaustion of the new extension twinning happening, which is also seen for other wrought Mg alloys at different strain amplitudes [16][27]. Finally, as seen in Figure 5(f), the second and half-life hysteresis loops at the strain amplitude of 0.7% show sigmoidal shapes indicating the activation of extension twin and detwining under compressive and tensile loading, respectively. Additionally, an investigation on the evolution of internal stress during the cyclic deformation by $\{10\bar{1}2\}\langle 10\bar{1}1\rangle$ extension twins in the extruded ZK60 reported that the local intergranular stress drives the activation of detwining [49], thereby detwinning along the c-axis is starting in the reverse tensile loading with small external stress at the stress of ~ -100 MPa.

Figure 6 shows the half-life hysteresis loops for the as-cast ZK60 for different strain amplitudes. It is noted that the shape of hysteresis loops as well as the peak stresses are symmetric in tension and compression reversals. This behavior is an evidence of slip being the dominant plastic deformation [26][50], which is attributed to the random texture in the cast Mg alloy. To be more specific, returning to the texture measurement (Figure 4(a)), ZK60 cast has no preferred unit cell orientation inside its microstructure. Therefore, extension twins will not take over during low deformation. Nevertheless, the hysteresis loop at the strain amplitude of 0.9% tends to be marginally sigmoidal shape, which is evidence for the mild activation of extension twins and detwinning at higher deformation levels. In fact, in a randomly textured material, some grains would have an orientation that is favorable for activation of twinning. As a result, at high strain amplitudes, some twining might happen for which the hysteresis loop would be sigmoidal;

ACCEPTED MANUSCRIPT

however, the hysteresis loop is still symmetric at the strain amplitude of 0.9%, as the amount of twinning may not be significant. Comparing with the half-life hysteresis loops in as-cast condition (Figure 6), the forged half-life hysteresis loops (Figure 7) exhibit asymmetric behavior above the strain amplitude of 0.4%.As seen in Figure 7, the hysteresis loops are almost symmetric up to the strain amplitude of 0.4% in terms of both the shape of hysteresis loop and the peak stresses. However, at the strain amplitudes higher than 0.4%, the hysteresis loops tend to be asymmetric. Such an asymmetric behavior stems from the strong basal texture developed during the forging process. According to Figure 2(b) and Figure 4(b), tensile loading on the fatigue specimen (along LD) applies contraction along the c-axis of HCP unit cells, then no twining occurs. However, compressive loading brings about extension along the c-axis, thereby twining takes over [47]. The twinning deformation is often characterized by very low hardening rates [48]. Thus, the strain hardening rate decreases by increasing the strain amplitude. On the other hand, under tensile loading, detwinning occurs inside the twinned grains which also accompanies with low strain hardening rate [51]. By contrast, following the detwining exhaustion, strain hardening rate increases dramatically. The increase in the hardening rate is attributed to the new orientation of HCP unit cells inside the grains of the alloy after detwinning that causes the activation of higher order non-basal slip systems, which has significantly higher critical resolved shear stress (CRSS), and compression twinning systems [52][53][54].

Figure 8 presents the cyclic tension and cyclic compression curves for the as-cast and cast-forged ZK60. The curves were obtained by connecting the peak stresses of the half-life hysteresis loops at different strain amplitudes. The tensile and compressive peak stresses for the as-cast alloy were almost similar in comparison to the forged alloy. For the forged alloy, however, the tensile peak stresses were higher than the compressive ones for strain amplitudes higher than 0.4%. This concurs well with Figure 6 and Figure 7 where symmetric and asymmetric cyclic behaviors were observed for the as-cast and forged samples, respectively.

The tensile quasi-static and cyclic behavior of as-cast and cast-forged alloys are depicted in Figure 9. It is noticed that at low strain values, the quasi-static and cyclic behaviors are approximately the same; however, with increasing the strain values, the cyclic curves become harder than the monotonic curves, which confirms the cyclic hardening behavior for the two materials. Figure 10(a) and (b) also show the evolution of stress amplitude during strain

ACCEPTED MANUSCRIPT

controlled test for the as-cast and forged ZK60, respectively. For the both conditions, as-cast and forged, the stress amplitude is almost constant at lower strain amplitudes up to 0.3%. However, stress amplitude has an increasing trend for higher strain amplitudes, which demonstrates cyclic hardening behavior. The variation of stress amplitude with the number of cycles has already been studied for extruded ZK60 [26]. The results for the extruded alloy were the same as the results of this study for the forged alloy. The stress amplitude did not change up to strain amplitude of 0.35%, it started to increase for the strain amplitudes of 0.4% and higher. It was also reported that increasing the loading cycles increased the dislocation density which act as barriers against the movement other dislocation which builds up the resistance to plastic deformation resulting in cyclic hardening [55][56]. Moreover, at higher strain amplitudes, and in particular for the forged alloy, twining is an active mode of deformation under compression loading. Twin deformations in the compressive reversal are partially reversed in the subsequent tensile reversal, but some residual twins remain. The interactions of dislocation-twin besides twin-twin brings about the strain hardening [47][55][57].

Figure 10(b) shows a drop in the stress amplitude at the strain amplitude of 0.9%. Also, in both Figure 8 and Figure 9, a decrease in the tensile peak stress is observed at the total strain amplitude of 0.9%. This behavior might be due to the micro-cracks formation near grain boundaries and twin tips, as has been previously observed for pure Mg [57]. With increasing strain amplitude, and accordingly the applied load, some micro-cracks may initiate inside the microstructure reducing the material's ability to endure tensile loading. On the contrary, the compressive peak stress has increased at the strain amplitude of 0.9% (as seen in Figure 8), which can be due to crack closure occurring. Hence, micro-cracks deteriorates the strength of material under tension but not under compression. Aside from this, the drop in the maximum tensile peak had already been seen for extruded ZK60 Mg alloy after the strain amplitude of 0.8% [26][27].

The number of cycles to failure, N_f, against the applied total strain amplitudes ($\Delta\varepsilon_t/2$) for the ZK60 Mg alloy in as-cast and forged conditions is depicted in Figure 11, along with some data available in literature for extruded ZK60 [25]. The as-cast alloy obtained lower fatigue life to that of the forged ZK60 Mg alloy at high strain amplitudes and significantly lower life compared to the forged alloy at low strain amplitudes. Also, the extruded ZK60 shows shorter

ACCEPTED MANUSCRIPT

fatigue life for the similar testing condition. It should be mentioned that the fatigue life is always higher in forged samples compared to the extruded materials above a total strain amplitude of 0.4%. Additionally, a couple of run-out tests were run to assess the strain amplitude leading to 10^7 cycles (run-out). The run-out life was achieved at the total strain amplitude of 0.175% for the as-cast alloy, while the forged ZK60 could endure higher strain amplitude of 0.22%, which confirms the improvement of HCF response. It is reported that the high cycle fatigue life is controlled by the strength of materials [35][58]. Therefore, it is believed that higher strength of the forged alloy compared to the as-cast alloy can lead to the superior fatigue strength in the HCF regime. Additionally, the presence of intermetallics in the microstructure can cause stress concentration, which facilitates crack nucleation. As explained earlier, the forged ZK60 contained less amount of porosities and intermetallics, which can contribute to the longer HCF life [58]. On the other hand, for strain amplitudes higher than 0.4%, twinning is active for the forged alloy due to the strong developed basal texture (as seen in Figure 4(b)). Twinned lamellas can be a zone for crack initiation leading into a premature fracture happening [57]. Moreover, the tension-compression asymmetry stemming from the induced texture (and not hydrostatic stress as is in the case of strength differential effect of high strength metals [59]) brings about tensile mean stress which affects the fatigue life adversely. Therefore, the similar fatigue lives for as-cast and forged ZK60 in the LCF regime might be due to combination of different factors: i) improvement of fatigue response as a result of grain refinement and lower density of porosities and intermetallics, ii) the adverse effects of strong basal texture induced during the forging process.

3.4 Fracture surface analysis

SEM images of the fatigue fracture surface of as-cast and cast-forged samples at two strain amplitudes of 0.5% and 0.9% are presented in Figure 12. Fatigue crack initiation (FCI), fatigue crack growth (FCG), and final fracture (FF) areas are demarcated as the main features of the fracture surface. It is clear that the forged samples tested at different strain amplitudes shows multiple FCI sites while the as-cast sample exhibits lower number of FCI sites. In general, increasing the strain amplitudes, the FCG zone decreased which is the indication of shorter fatigue life as seen in Figure 11. At the same time, a wider FCG zone can be detected on the

ACCEPTED MANUSCRIPT

fracture surface of the forged sample compared to the as-cast sample indicating the longer fatigue life of the forged sample. This can be due to the fact that the microstructure of the forged alloy contains finer grains and also that less volume fraction of porosities and inclusions exists in the material (Figure 3). Figure 13 depicts the crack initiation site of the as-cast alloy at higher magnifications. Most of the cracks have initiated from the open surface area as a consequence of the extrusion/intrusion of the slip bands formation, known as persistent slip band (PSB), or casting porosities. These porosities can join together and make voids leading to a crack formation. At the same time, the interactions between grains and PSB, which are made by cyclic irreversible slips, are reported to be a major drive for crack initiation in different metals, especially in HCF regime [60][61][62]. However, other studies [63] also stated that in the LCF regime, crack initiation and propagation proceed along PSB through dendritic cells in the as-cast alloys as well. Figure 14 shows the crack initiation sites of the forged alloy at the similar two total strain amplitudes at higher magnifications. As shown in Figure 14 (b), oxide layers are observed on the FCI sites. It is also noticed that the matrix was delaminated and formed a step like morphology during crack propagation. In addition, secondary cracks were also noticed in the matrix which is an indication of strengthening of the matrix (Figure 14(d)). As seen in Figure 15, micro-cliffs, step like morphologies parallel to the fatigue cracks, and fatigue striation (FS) are the main characteristics which are marked by arrows of the FCG zone. It is well established that the fatigue cracks are propagating perpendicular to the FS and parallel to the micro-cliffs [64]. Each striation mark denotes the fatigue crack propagation in each cycle. It is noticed that the FS marks on the fracture surface of the forged alloy are finer than those on the surface of as-cast alloy under the same strain amplitude. For instance, at the total strain amplitude of 0.5%, the average distance between the striations on the fracture surface of as-cast ZK60 is ~1.2 µm, while the forged material exhibits FS with average distance of ~0.65 µm. This corresponds well with the longer fatigue life of the forged alloy. At the same time, it is noticed that with increasing the strain amplitude (Figure 15(b) and Figure 15(d)), FS marks become coarser (~2.6 µm and 0.9 µm between the striations for the as-cast and forged ZK60, respectively, at the total strain amplitude of 0.9%) because more cracks opening lead to greater plasticity on each cycle. Figure 16 represents the magnified FF zones on the fatigue fracture surface of the as-cast and forged ZK60. It is worth to mention that FF area for all testing conditions show tensile like morphology as illustrated in [39]. As depicted in Figure 16, the as-cast alloy resembles a quasi-cleavage surface

ACCEPTED MANUSCRIPT

with some dimples besides tear ridges. In contrast, more dimples can be observed on the fracture surface of the forged alloy. This is in correlation with the result obtained under tensile monotonic results (Table 1) that the forged alloy exhibits higher ductility. At the same time, the SEM images at the FF evident that intermetallics played a great roll in fatigue life (Figure 17). As discussed earlier that the volume fraction of intermetallics in the as-cast sample is higher than the forged sample (Figure 3). As displayed in Figure 17(a, b), the identified intermetallics on the fracture surfaces of as-cast samples tested at the different stress amplitude of 0.5% and 0.9% were $ZnZr_2$ and $MgZn_2$, which exhibits multiple cracks were the potential sites of the nucleation of cracks results premature failure and shorter the fatigue life. In contrast, the fracture surfaces of forged samples (Figure 17(c, d)) tested at the similar strain amplitudes shows less volume fraction of the intermetallic (only $ZnZr_2$) results lower nucleation sites for the cracks leading to the longer fatigue life. The combined action of grain refinement, modification of texture and strengthening of the matrix by dissolving the intermetallics (solid solution strengthening) and reducing the defects has caused the forged sample to obtain longer fatigue life compared to the as-cast ZK60. Similar type of fatigue life enhancement was observed in cast forged AZ31B [38].

3.5 Fatigue modeling

Fatigue is the primary failure mechanism in most engineering components hence the accurate prediction of the fatigue life of an in-service component is of critical importance. Several fatigue models were established to predict the fatigue life leading to the fatigue damage per cycle and compared with the experimental obtained fatigue life data [65]–[68]. The suggested models are either stress- strain- or energy-based. In this study, the stress based approached may not be suitable for modelling the ZK60 alloy subjected to strain-controlled fatigue testing [69]. At the same time, the well-established fatigue models presently available in literature were either for isotropic materials, or for other forms of wrought Mg alloys (such as rolling or extrusions) with different characteristics than the current forged ZK60 alloy. Therefore the present study adopted the following models to describe the cyclic behavior of the studied ZK60 alloy.

The strain-life response of metals is often modeled by Coffin-Manson-Basquin (Morrow's) equation [70][71]. The elastic strain and plastic strain amplitudes are defined by the Basquin and Coffin-Manson equations, respectively as:

ACCEPTED MANUSCRIPT

$$\varepsilon_{a,elastic} = \frac{\sigma_f'}{E}(2N_f)^b \quad (1)$$

$$\varepsilon_{a,plastic} = \varepsilon_f'(2N_f)^c \quad (2)$$

where, $\varepsilon_{a,elastic}$ and $\varepsilon_{a,plastic}$ are the elastic and plastic strain amplitudes, respectively. E is the modulus of elasticity, which is approximately 45 GPa for ZK60 Mg alloy [67] and close to the average modulus of elasticity obtained from cyclic tests, and N_f is the fatigue life. σ_f' and b are the fatigue strength coefficient and fatigue strength exponent, respectively, and ε_f' and c are fatigue ductility coefficient and fatigue ductility exponent, respectively. The total strain amplitude, ε_a, is then obtained from:

$$\varepsilon_a = \frac{\sigma_f'}{E}(2N_f)^b + \varepsilon_f'(2N_f)^c \quad (3)$$

Eq. (1) and (2) were employed to calculate the Coffin-Manson Parameters which are listed in Table 3. Figure 18 represents the fatigue life predicted by the Coffin-Manson model versus the life obtained from the experiments. According to this figure, the majority of data points are located between the factor of 2 bound lines. However, two data points corresponding to $\varepsilon_a = 0.25\%$ lay outside this domain.

The Jahed-Varvani model (JV) [72] [73] was also employed in this study to predict the fatigue life of as-cast and forged ZK60. The JV model relates the fatigue life to a measure of strain energy, as opposed to the Coffin-Manson model relating the life to strain amplitude. The JV model accounts for the mean stress effects. Because energy is a scalar parameter, the strain energy corresponding to different stress/strain components can be manipulated algebraically, without the concern of different material orientation or loading direction [67]. According to this model, the total strain energy density is expressed by two terms: i) the positive elastic strain energy density, ΔE_e^+, and ii) the plastic strain energy density, ΔE_p [74]. The former part which accounts for the effect of mean stress can be calculated by Eq. 4, where σ_{max} is the tensile peak stress of the hysteresis loop. In addition, the plastic strain energy density is calculated from the area inside the half-life hysteresis loop.

$$\Delta E_e^+ = \frac{\sigma_{max}^2}{2E} \quad (4)$$

ACCEPTED MANUSCRIPT

Figure 19 displays the schematic of the total energy density obtained from the half-life hysteresis loop.

The strain energy density is then related to the fatigue life as:

$$\Delta E = E'_e(2N_f)^B + E'_f(2N_f)^C \quad (5)$$

where E'_e, B, E'_f, and C are the fatigue strength coefficient, the fatigue strength exponent, the fatigue toughness coefficient, and the fatigue toughness exponent, respectively. The values of these parameters are calculated and listed in Table 4.

Figure 20 displays the correlation between the predicted fatigue life and the experimentally obtained fatigue life of the as-cast and forged materials. As can be seen, the majority of the data points are banded within the lines of factor of 1.5 which shows the promise of JV model to predict the fatigue life of as-cast and forged ZK60 under uniaxial loading.

There was more scatter seen in the Coffin-Manson results due to the fact that Coffin-Manson equation does not account for the mean stress effect, whereas mean stress are generated during fully reversed strain-controlled tests due to asymmetry. However, in the JV model, as indicated previously, the elastic part of the total strain energy density accounts for the means stress effect. .

4. Conclusions

In the present study, the cyclic behavior of as-cast and cast-forged ZK60 was studied at different strain amplitudes. From the above results and discussion, the following conclusions are made:

1- While as-cast ZK60 displays symmetric hysteresis loops at different strain amplitudes, the shape of hysteresis loops for the forged material depends on the applied strain amplitude. For the strain amplitudes lower than 0.4%, the shape of the hysteresis loops is symmetric and dislocation slip governs the deformation. At the strain amplitude of 0.4%-0.5%, twinning is activated under the compression reversal and detwinning occurs during

ACCEPTED MANUSCRIPT

the subsequent tension reversal during the first few cycles; therefore, the hysteresis loop shape is sigmoidal. However, the half-life hysteresis loop is symmetric, as no more twinning/ detwinning is happening. For strain amplitudes more than 0.5%, the applied stress is large enough to make twinning/ detwinning occurring during the whole life as a result of the basal texture, thereby the half-life hysteresis loop as well as the second cycle hysteresis loop is asymmetric.

2- In general, forged ZK60 is exhibiting superior fatigue strength compared to the as-cast alloy owing to the grain refinement happening in the forged material and lower amount of porosities and second-phase particles inside its microstructure.
3- Different mechanisms of crack initiation for the forged material are proposed. At high cycle fatigue regime, persistent slip bands (PSB) and intermetallics are the major cause of crack nucleation. On the other hand, for the strain amplitudes higher than 0.4%-0.5%, that twinning is occurring, the interaction between twin-twin bands besides twin-dislocation can also form cracks leading to final fracture.
4- The Coffin-Manson fatigue model and the energy-based JV model were assessed in terms of the fatigue life prediction for the as-cast and forged ZK60. Both models yielded predictions with the 2x band, however, due to consideration of mean stress through elastic strain energy density, the JV model predictions were confined within 1.5x band.

Acknowledgment

This work is financially supported by the Natural Sciences and Engineering Research Council of Canada, the Automotive Partnership Canada (APC) program under APCPJ 459269-13 grant with contributions from Multimatic Technical Centre, Ford Motor Company, and Centerline Windsor. The authors would also like to thank Jonathan McKinley and Lucian Blaga of CanmetMATERIALS for the forgings.

References

ACCEPTED MANUSCRIPT

[1] W. S. Miller, L. Zhuang, J. Bottema, A. J. Wittebrood, and P. De Smet, "Recent development in aluminium alloys for the automotive industry," *Mater. Sci. Eng. A*, vol. 280, no. 1, pp. 37–49, 2000.

[2] H. Friedrich and S. Schumann, "Research for a 'new age of magnesium' in the automotive industry," *J. Mater. Process. Technol.*, vol. 117, no. 3, pp. 276–281, 2001.

[3] B. L. Mordike and T. Ebert, "Magnesium Properties - applications - potential," *Mater. Sci. Eng. A*, vol. 302, no. 1, pp. 37–45, 2001.

[4] D. Eliezer, E. Aghion, and F. H. Froes, "Magnesium science, technology and applications," *Adv. Perform. Mater.*, vol. 5, no. 3, pp. 201–212, 1998.

[5] M. Easton, A. Beer, M. Barnett, C. Davies, and G. Dulop, "Magnesium Alloy Applications in Automotive Structures," *JOM*, vol. 60, no. 11, pp. 57–60, 2008.

[6] M. K. Kulekci, "Magnesium and its alloys applications in automotive industry," *Int. J. Adv. Manuf. Technol.*, vol. 39, no. 9–10, pp. 851–865, 2008.

[7] R. von Mises, "Mechanik der plastischen Formanderung von Kristallen," *ournal Appl. Math. Mech. für Angew. Math. und Mech.*, vol. 8, no. 3, pp. 161–185, 1928.

[8] E. Meza-garc, P. Dobroˇ, J. Bohlen, D. Letzig, and K. Ulrich, "Deformation mechanisms in an AZ31 cast magnesium alloy as investigated by the acoustic emission technique," *Mater. Sci. Eng. A*, vol. 462, no. 1–2, pp. 297–301, 2007.

[9] S. R. Agnew and Ö. Duygulu, "Plastic anisotropy and the role of non-basal slip in magnesium alloy AZ31B," *Int. J. Plast.*, vol. 21, no. 6, pp. 1161–1193, 2005.

[10] X. Y. Lou and M. Li, "Hardening evolution of AZ31B Mg sheet," *Int. J. Plast.*, vol. 23, pp. 44–86, 2007.

[11] D. W. Brown, A. Jain, S. R. Agnew, and B. Clausen, "Twinning and Detwinning During Cyclic Deformation of Mg Alloy AZ31B," *Mater. Sci. Forum*, vol. 539–543, pp. 3407–3413, 2007.

[12] T. Al-Samman and G. Gottstein, "Dynamic recrystallization during high temperature deformation of magnesium," *Mater. Sci. Eng. A*, vol. 490, no. 1–2, pp. 411–420, 2008.

[13] A. Chapuis and J. H. Driver, "Temperature dependency of slip and twinning in plane strain compressed magnesium single crystals," *Acta Mater.*, vol. 59, no. 5, pp. 1986–1994, 2011.

[14] F. Pan, M. Yang, and X. Chen, "A Review on Casting Magnesium Alloys : Modification of Commercial Alloys and Development of New Alloys," *J. Mater. Sci. Technol.*, vol. 32, no. 12, pp. 1211–1221, 2016.

[15] H. Mayer, M. Papakyriacou, B. Zettl, and S. E. Stanzl-tschegg, "Influence of porosity on the fatigue limit of die cast magnesium and aluminium alloys," *Int. J. Fatigue*, vol. 25, pp. 245–256, 2003.

[16] A. A. Roostaei and H. Jahed, "Role of loading direction on cyclic behaviour characteristics of AM30 extrusion and its fatigue damage modelling," *Mater. Sci. Eng. A*,

ACCEPTED MANUSCRIPT

vol. 670, pp. 26–40, 2016.

[17] J. Albinmousa, H. Jahed, and S. Lambert, "Cyclic behaviour of wrought magnesium alloy under multiaxial load," *Int. J. Fatigue*, vol. 33, no. 8, pp. 1127–1139, 2011.

[18] A. A. Roostaei and H. Jahed, "Multiaxial cyclic behaviour and fatigue modelling of AM30 Mg alloy extrusion," *Int. J. Fatigue*, vol. 97, pp. 150–161, 2017.

[19] Y. Estrin and A. Vinogradov, "Extreme grain refinement by severe plastic deformation: A wealth of challenging science," *Acta Mater.*, vol. 61, no. 3, pp. 782–817, 2013.

[20] S. R. Agnew, J. A. Horton, T. M. Lillo, and D. W. Brown, "Enhanced ductility in strongly textured magnesium produced by equal channel angular processing," *Scr. Mater.*, vol. 50, no. 3, pp. 377–381, 2004.

[21] C. Bettles and M. Gibson, "Current wrought magnesium alloys: Strengths and weaknesses," *Jom*, vol. 57, no. 5, pp. 46–49, 2005.

[22] J. D. Robson and C. Paa-Rai, "The interaction of grain refinement and ageing in magnesium–zinc–zirconium (ZK) alloys," *Acta Mater.*, vol. 95, pp. 10–19, 2015.

[23] J. S. Chun and J. G. Byrne, "Precipitate Sterngthening Mechanisms in Magnesium Zinc Alloy Single Crystal," *J. Mater. Sci.*, vol. 4, pp. 861–872, 1969.

[24] W. C. Liu, J. Dong, P. Zhang, Z. Y. Yao, C. Q. Zhai, and W. J. Ding, "High cycle fatigue behavior of as-extruded ZK60 magnesium alloy," *J. Mater. Sci.*, vol. 44, no. 11, pp. 2916–2924, 2009.

[25] Y. Xiong and Y. Jiang, "Fatigue of ZK60 magnesium alloy under uniaxial loading," *Int. J. Fatigue*, vol. 64, pp. 74–83, 2014.

[26] Y. Xiong, Q. Yu, and Y. Jiang, "An experimental study of cyclic plastic deformation of extruded ZK60 magnesium alloy under uniaxial loading at room temperature," *Int. J. Plast.*, vol. 53, pp. 107–124, 2014.

[27] Q. Yu, J. Zhang, Y. Jiang, and Q. Li, "An experimental study on cyclic deformation and fatigue of extruded ZK60 magnesium alloy," *Int. J. Fatigue*, vol. 36, no. 1, pp. 47–58, 2012.

[28] R. Jahadi, M. Sedighi, and H. Jahed, "ECAP effect on the micro-structure and mechanical properties of AM30 magnesium alloy," *Mater. Sci. Eng. A*, vol. 593, pp. 178–184, 2014.

[29] S. R. Agnew, P. Mehrotra, T. M. Lillo, G. M. Stoica, and P. K. Liaw, "Texture evolution of five wrought magnesium alloys during route a equal channel angular extrusion: Experiments and simulations," *Acta Mater.*, vol. 53, no. 11, pp. 3135–3146, 2005.

[30] S. H. Park, S. G. Hong, W. Bang, and C. S. Lee, "Effect of anisotropy on the low-cycle fatigue behavior of rolled AZ31 magnesium alloy," *Mater. Sci. Eng. A*, vol. 527, no. 3, pp. 417–423, 2010.

[31] S. Hasegawa, Y. Tsuchida, H. Yano, and M. Matsui, "Evaluation of low cycle fatigue life in AZ31 magnesium alloy," *Int. J. Fatigue*, vol. 29, no. 9–11, pp. 1839–1845, 2007.

ACCEPTED MANUSCRIPT

[32] M. Madaj, M. Greger, and V. Karas, “MAGNESIUM-ALLOY DIE FORGINGS FOR AUTOMOTIVE APPLICATIONS,” *Mater. Tehnol.*, vol. 49, no. 2, pp. 267–273, 2015.

[33] G. Yu, “Forging Specimen Design for Magnesium Alloys,” *(Master’s Thesis), Retrieved from Univ. Waterloo Database*, 2016.

[34] D. Toscano, S. K. Shaha, B. Behravesh, H. Jahed, M. Wells, B. Williams, and J. McKinley, “Effect of Forging on Microstructure, Texture and Compression Behavior of Extruded AZ31B,” in *Proceedings of the 3rd Pan American Materials Congress*, Springer International Publishing, 2017, pp. 347–354.

[35] E. Vasilev, M. Linderov, D. Nugmanov, O. Sitdikov, M. Markushev, and A. Vinogradov, “Fatigue Performance of Mg-Zn-Zr Alloy Processed by Hot Severe Plastic Deformation,” *Metals (Basel).*, vol. 5, no. 4, pp. 2316–2327, 2015.

[36] A. Gryguc, S. K. Shaha, S. B. Behravesh, H. Jahed, M. Wells, B. Williams, and X. Su, “Monotonic and cyclic behaviour of cast and cast-forged AZ80 Mg,” *Int. J. Fatigue*, vol. 104, pp. 136–149, 2017.

[37] A. Gryguc, S.K. Shaha, H. Jahed, M. Wells, B. Williams, J. McKinley, “Tensile and fatigue behaviour of as-forged AZ31B extrusion,” *Fract. Struct. Integr.*, vol. 38, pp. 251–258, 2016.

[38] D. Toscano, S. K. Shaha, B. Behravesh, H. Jahed, and B. Williams, “Effect of forging on the low cycle fatigue behavior of cast AZ31B alloy,” *Mater. Sci. Eng. A*, vol. 706, no. May, pp. 342–356, 2017.

[39] S. M. H. Karparvarfard, S. K. Shaha, S. B. Behravesh, H. Jahed, and B. W. Williams, “Microstructure , texture and mechanical behavior characterization of hot forged cast ZK60 magnesium alloy,” *J. Mater. Sci. Technol.*, 2017.

[40] W. Yu, Z. Liu, H. He, N. Cheng, and X. Li, “Microstructure and mechanical properties of ZK60 – Yb magnesium alloys,” *Mater. Sci. Eng. A*, vol. 478, no. 1–2, pp. 101–107, 2008.

[41] A. Hadadzadeh, S. K. Shaha, M. A. Wells, H. Jahed, and B. Williams, “Recrystallization behavior and texture evolution during hot deformation of extruded ZK60 magnesium alloy,” in *Conference: Materials Science and Technology 2016, MS&T 2016, Location Salt Lake City, UT, USA, Date: Oct 23-27*, 2016, pp. 281–288.

[42] S. M. H. Karparvarfard, S. K. Shaha, A. Hadadzadeh., S. B. Behravesh, H. Jahed, M. A. Wells, and B. Williams, “Characterization of Semi-Closed Die-Forged ZK60 Mg Alloy Extrusion,” *Magnes. Technol. 2017*, pp. 329–334, 2017.

[43] D. Toscano, S. . Shaha, S. B. Behravesh, H. Jahed, M. A. Wells, B. W. Williams, and J. McKinley, “Effect of Forging on Microstructure, Texture and Uniaxial Properties of Cast AZ31B Alloy,” *J. Mater. Eng. Perform.*, vol. 26, no. 7, pp. 3090–3103, 2017.

[44] J. B. Jordon, J. B. Gibson, M. F. Horstemeyer, H. El Kadiri, J. C. Baird, and A. A. Luo, “Effect of twinning, slip, and inclusions on the fatigue anisotropy of extrusion-textured AZ61 magnesium alloy,” *Mater. Sci. Eng. A*, vol. 528, no. 22–23, pp. 6860–6871, 2011.

[45] S. K. Shaha, F. Czerwinski, W. Kasprzak, and D. L. Chen, “Tensile and compressive

ACCEPTED MANUSCRIPT

deformation behavior of the Al-Si-Cu-Mg cast alloy with additions of Zr, V and Ti," *Mater. Des.*, vol. 59, pp. 352–358, 2014.

[46] W. R. Osorio, P. R. Goulart, S. G. A, N. C. Moura, and A. Garcia, "Effect of Dendritic Arm Spacing on Mechanical Properties and Corrosion Resistance of Al 9 Wt Pct Si and Zn 27 Wt Pct Al Alloys," *Metall. Mater. Trans. A*, vol. 37, pp. 2525–2538, 2006.

[47] L. Wu, A. Jain, D. W. Brown, G. M. Stoica, S. R. Agnew, B. Clausen, D. E. Fielden, and P. K. Liaw, "Twinning–detwinning behavior during the strain-controlled low-cycle fatigue testing of a wrought magnesium alloy, ZK60A," *Acta Mater.*, vol. 56, no. 4, pp. 688–695, 2008.

[48] S. R. Agnew and and J. J. B. Christopher A. Calhoun, "What is in a Strain Hardening 'Plateau'?," in *Magnesium Technology 2016, Springer International Publishing*, 2016, pp. 189–194.

[49] L. Wu, S. R. Agnew, D. W. Brown, G. M. Stoica, B. Clausen, A. Jain, D. E. Fielden, and P. K. Liaw, "Internal stress relaxation and load redistribution during the twinning–detwinning-dominated cyclic deformation of a wrought magnesium alloy, ZK60A," *Acta Mater.*, vol. 56, no. 14, pp. 3699–3707, 2008.

[50] S. Kim, S. Hong, J. Lee, C. Soo, J. Yoon, and H. Yu, "Materials Science & Engineering A Anisotropic in-plane fatigue behavior of rolled magnesium alloy with { 10 − 12 } twins," *Mater. Sci. Eng. A*, vol. 700, no. May, pp. 191–197, 2017.

[51] X. Z. Lin and D. L. Chen, "Strain controlled cyclic deformation behavior of an extruded magnesium alloy," *Mater. Sci. Eng. A*, vol. 496, pp. 106–113, 2008.

[52] S. R. Agnew, M. H. Yoo, and C. N. Tomé, "Application of texture simulation to understanding mechanical behavior of Mg and solid solution alloys containing Li or Y," *Acta Mater.*, vol. 49, no. 20, pp. 4277–4289, 2001.

[53] Z. Keshavarz and M. R. Barnett, "EBSD analysis of deformation modes in Mg-3Al-1Zn," *Scr. Mater.*, vol. 55, no. 10, pp. 915–918, 2006.

[54] S. R. Agnew, D. W. Brown, and C. N. Tomé, "Validating a polycrystal model for the elastoplastic response of magnesium alloy AZ31 using in situ neutron diffraction," *Acta Mater.*, vol. 54, no. 18, pp. 4841–4852, 2006.

[55] G. Proust, C. N. Tomé, A. Jain, and S. R. Agnew, "Modeling the effect of twinning and detwinning during strain-path changes of magnesium alloy AZ31," *Int. J. Plast.*, vol. 25, no. 5, pp. 861–880, 2009.

[56] N. a. Fleck, G. M. Muller, M. F. Ashby, and J. W. Hutchinson, "Strain gradient plasticity: Theory and experiment," *Acta Metall. Mater.*, vol. 42, no. 2, pp. 475–487, 1994.

[57] Q. Yu, J. Zhang, and Y. Jiang, "Fatigue damage development in pure polycrystalline magnesium under cyclic tension-compression loading," *Mater. Sci. Eng. A*, vol. 528, no. 25–26, pp. 7816–7826, 2011.

[58] Y. Estrin and A. Vinogradov, "Fatigue behaviour of light alloys with ultrafine grain structure produced by severe plastic deformation : An overview," *Int. J. Fatigue*, vol. 32,

ACCEPTED MANUSCRIPT

no. 6, pp. 898–907, 2010.

[59] J. Casey and H. Jahedmotlagh, “THE STRENGTH-DIFFERENTIAL EFFECT IN PLASTICITY,” *Int. J. Solids Struct.*, vol. 20, no. 4, pp. 377–393, 1984.

[60] H. Mughrabi, R. Wang, K. Differt, and C. Fatigue, “Fatigue Crack Initiation by Cyclic Slip Irreversibilities in High-Cycle Fatigue,” *Fatigue Mech. Adv. Quant. Meas. Phys. Damage, STP30551S, J. Lankford, D. Davidson, W. Morris, R. Wei, Ed., ASTM Int. West Conshohocken, PA*, pp. 5–45, 1983.

[61] U. Essmann, U. Gösele, and H. Mughrabi, “A model of extrusions and intrusions in fatigued metals I . Point-defect production and the growth of extrusions,” *Philos. Mag. A*, vol. 44, no. 2, pp. 405–426, 1981.

[62] K. Gall, G. Biallas, H. J. Maier, P. Gullett, M. F. Horstemeyer, D. L. Mcdowell, and J. Fan, “In-situ observations of high cycle fatigue mechanisms in cast AM60B magnesium in vacuum and water vapor environments,” *Int. J. Fatigue*, vol. 26, pp. 59–70, 2004.

[63] K. E. N. Gall, G. Biallas, H. J. Maier, P. Gullett, M. F. Horstemeyer, and D. L. Mcdowell, “In-Situ Observations of Low-Cycle Fatigue Damage in Cast AM60B Magnesium in an Environmental Scanning Electron Microscope METHODS,” *Metall. Mater. Trans. A*, vol. 35, no. January, pp. 321–331, 2004.

[64] S. K. Shaha, F. Czerwinski, W. Kasprzak, J. Friedman, and D. L. Chen, “Monotonic and cyclic deformation behavior of the Al-Si-Cu-Mg cast alloy with micro-additions of Ti, V and Zr,” *Int. J. Fatigue*, vol. 70, 2015.

[65] K. N. Smith, P. Watson, and T. H. Topper, “Stress-Strain Function for the Fatigue of Metals,” *Journal of Materials*, vol. 5. pp. 767–778, 1970.

[66] J. Albinmousa and H. Jahed, “Multiaxial effects on LCF behaviour and fatigue failure of AZ31B magnesium extrusion,” *Int. J. Fatigue*, vol. 67, pp. 103–116, 2014.

[67] H. Jahed and J. Albinmousa, “Multiaxial behaviour of wrought magnesium alloys – A review and suitability of energy-based fatigue life model,” *Theor. Appl. Fract. Mech.*, vol. 73, pp. 97–108, 2014.

[68] J. Dallmeier, O. Huber, H. Saage, and K. Eigenfeld, “Uniaxial cyclic deformation and fatigue behavior of AM50 magnesium alloy sheet metals under symmetric and asymmetric loadings,” *Mater. Des.*, vol. 70, pp. 10–30, 2015.

[69] Y. C. Lin, Z. H. Liu, X. M. Chen, and J. Chen, “Stress-based fatigue life prediction models for AZ31B magnesium alloy under single-step and multi-step asymmetric stress-controlled cyclic loadings,” *Comput. Mater. Sci.*, vol. 73, pp. 128–138, 2013.

[70] J. Dallmeier, O. Huber, H. Saage, K. Eigenfeld, and A. Hilbig, “Quasi-static and fatigue behavior of extruded ME21 and twin roll cast AZ31 magnesium sheet metals,” *Mater. Sci. Eng. A*, vol. 590, pp. 44–53, 2014.

[71] S. Begum, D. L. Chen, S. Xu, and A. A. Luo, “Low cycle fatigue properties of an extruded AZ31 magnesium alloy,” *Int. J. Fatigue*, vol. 31, no. 4, pp. 726–735, 2009.

ACCEPTED MANUSCRIPT

[72] H. Jahed and A. Varvani-farahani, "Upper and lower fatigue life limits model using energy-based fatigue properties," *Int. J. Fatigue*, vol. 28, pp. 467–473, 2006.

[73] H. Jahed, A. Varvani-farahani, M. Noban, and I. Khalaji, "An energy-based fatigue life assessment model for various metallic materials under proportional and non-proportional loading conditions," *Int. J. Fatigue*, vol. 29, pp. 647–655, 2007.

[74] F. Ellyin, K. Golos, and Z. Xia, "In-Phase and Out-of-Phase Multiaxial Fatigue," *J. Eng. Mater. Technol.*, vol. 113, no. 1, pp. 112–118, 1991.

ACCEPTED MANUSCRIPT

ACCEPTED MANUSCRIPT

Table Captions:

Table 1. Mechanical properties of as-cast and forged ZK60 under monotonic tensile loading

Table 2. Cyclic tests summary for the half-life cycle for as-cast and forged ZK60 Mg alloy

Table 3. Coffin-Manson parameters for the as-cast and cast-forged ZK60 magnesium alloy

Table 4. The energy parameters of JV fatigue model for the tested as-cast and cast-forged ZK60 magnesium alloy

ACCEPTED MANUSCRIPT

ACCEPTED MANUSCRIPT

Figure Captions:

Figure 1. (a) Schematic illustration of the open-die forging process; (b) the final ZK60 sample after forging at 450^0C with the ram speed of 390 mm/min Note: LD-longitudinal direction, RD-radial direction and FD-forging direction.

Figure 2. Schematic depiction of the specimen locations and directions in (a) as-cast and (b) forged ZK60

Figure 3 Typical optical microstructures of as-cast ZK60 in unetched (a), and etched conditions (b) and forged ZK60 in unetched (c) and etched conditions (d)

Figure 4. The (0002) basal and $(10\bar{1}0)$ prismatic pole figures (PF) for (a) as-cast ZK60, (b) cast-forged ZK60 Mg alloy [39]

Figure 5. Typical engineering stress-engineering strain hysteresis loops for the as-cast (a, b, c) and forged (d, e, f) ZK60 Mg alloy at different total strain amplitudes of 0.3% (a, d), 0.5% (b, e), and 0.7% (c, f)

Figure 6. Half-life hysteresis loops for as-cast ZK60 obtained from fully-reversed strain controlled fatigue tests at different strain amplitudes of (a) 0.2 -0.5% and (b) 0.6-0.9%.

Figure 7. Half-life hysteresis loops for forged ZK60 obtained from fully-reversed strain controlled fatigue tests at different strain amplitudes of (a) 0.2 -0.4% and (b) 0.5-0.9%.

Figure 8. Cyclic behavior of as-cast and forged ZK60 obtained by connecting the peak stresses of the half-life hysteresis loops at different strain amplitudes. Note: T is for tensile peaks on and C is for compressive peaks

Figure 9. Comparison of the cyclic tensile and quasi-static tensile behavior for as-cast and forged ZK60

Figure 10. The variation of stress amplitude vs. number of cycles for (a) as-cast and (b) forged ZK60 under different strain amplitudes

Figure 11. Strain-life data obtained from fully-reversed strain controlled cyclic tests for cast and cast-forged ZK60

Figure 12. SEM images of fatigue fracture surfaces of ZK60 Mg alloy at different strain amplitudes (a) as-cast at ε_a =0.5%, (b) as-cast at ε_a =0.9%, (c) forged at ε_a =0.5%, and (d) forged at ε_a =0.9% (Yellow arrows indicate the position of FCI sites, and the dashed lines represent the boundary between the FCG and the FF zones)

Figure 13. SEM images of FCI locations in as-cast ZK60 tested at strain amplitudes of ε_a=0.5% (a-c), and ε_a=0.9% (d, e)

Figure 14. SEM images of fatigue fracture surfaces for cast forged ZK60 tested at a strain amplitude of 0.5% (a, b) and 0.9% (c, d) showing the crack initiation sites with (d) secondary cracks and delamination of the matrix.

ACCEPTED MANUSCRIPT

Figure 15. SEM images of the FCG regions of ZK60 under different strain amplitudes (a) as-cast at ε_a=0.5%, (b) as-cast at ε_a=0.9%, (c) forged at ε_a=0.5%, and (d) forged at ε_a=0.9%

Figure 16. SEM images of the FF regions of ZK60 under different strain amplitudes (a) as-cast at ε_a=0.5%, (b) as-cast at ε_a=0.9%, (c) forged at ε_a=0.5%, and (d) forged at ε_a=0.9%

Figure 17. SEM images with EDX spectrums of the FF regions of ZK60 under different strain amplitudes (a) as-cast at ε_a =0.5%, (b) as-cast at ε_a =0.9%, (c) forged at ε_a =0.5%, and (d) forged at ε_a =0.9%

Figure 18. Predicted life vs. experimental life for as-cast and forged ZK60 Mg alloy using the Coffin-Manson model

Figure 19. Schematic illustration of positive elastic and plastic strain energy densities [74]

Figure 20. Predicted life versus the experimental life for as-cast and forged ZK60 Mg alloy using the JV fatigue model

ACCEPTED MANUSCRIPT

ACCEPTED MANUSCRIPT

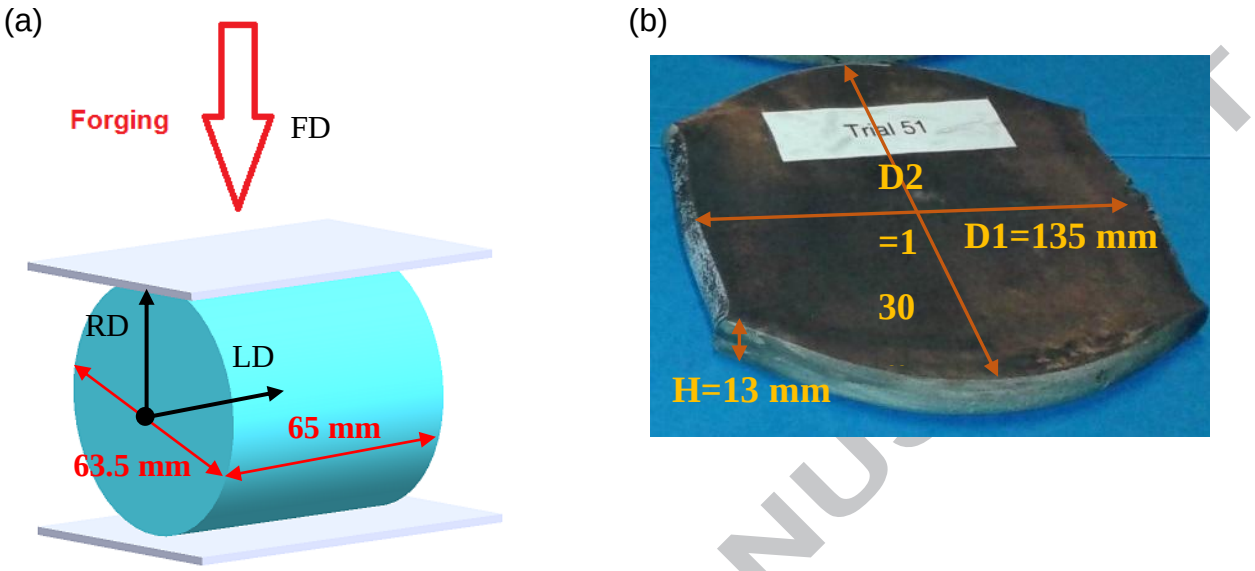

Figure 1. (a) Schematic illustration of the open-die forging process; (b) the final ZK60 sample after forging at 450°C with the ram speed of 390 mm/min

Note: LD-longitudinal direction, RD-radial direction, and FD-forging direction.

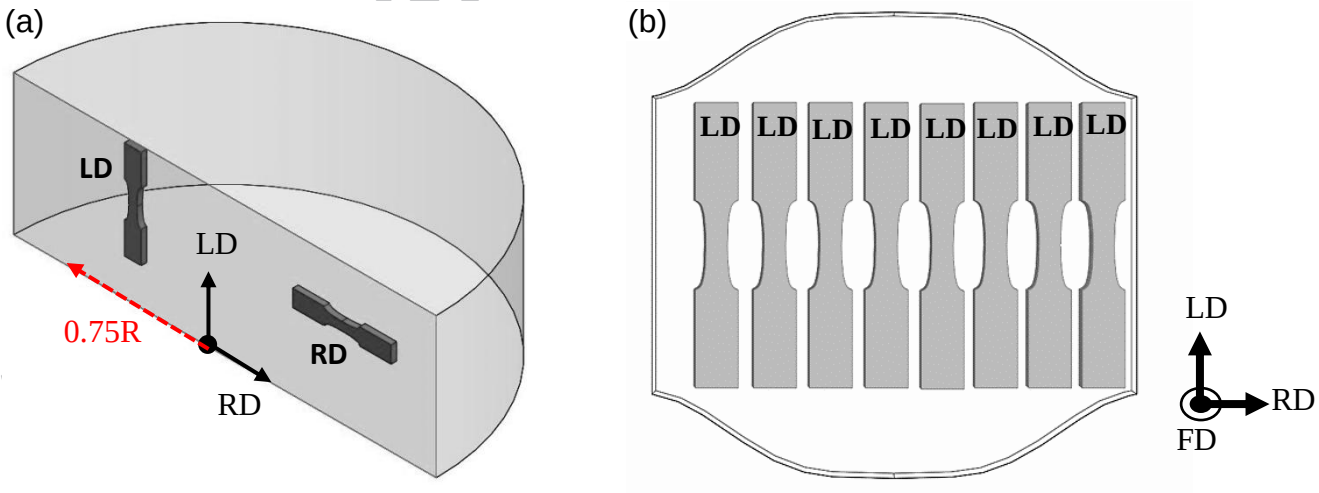

Figure 2. Schematic depiction of the specimen locations and directions in (a) as-cast and (b) forged ZK60

ACCEPTED MANUSCRIPT

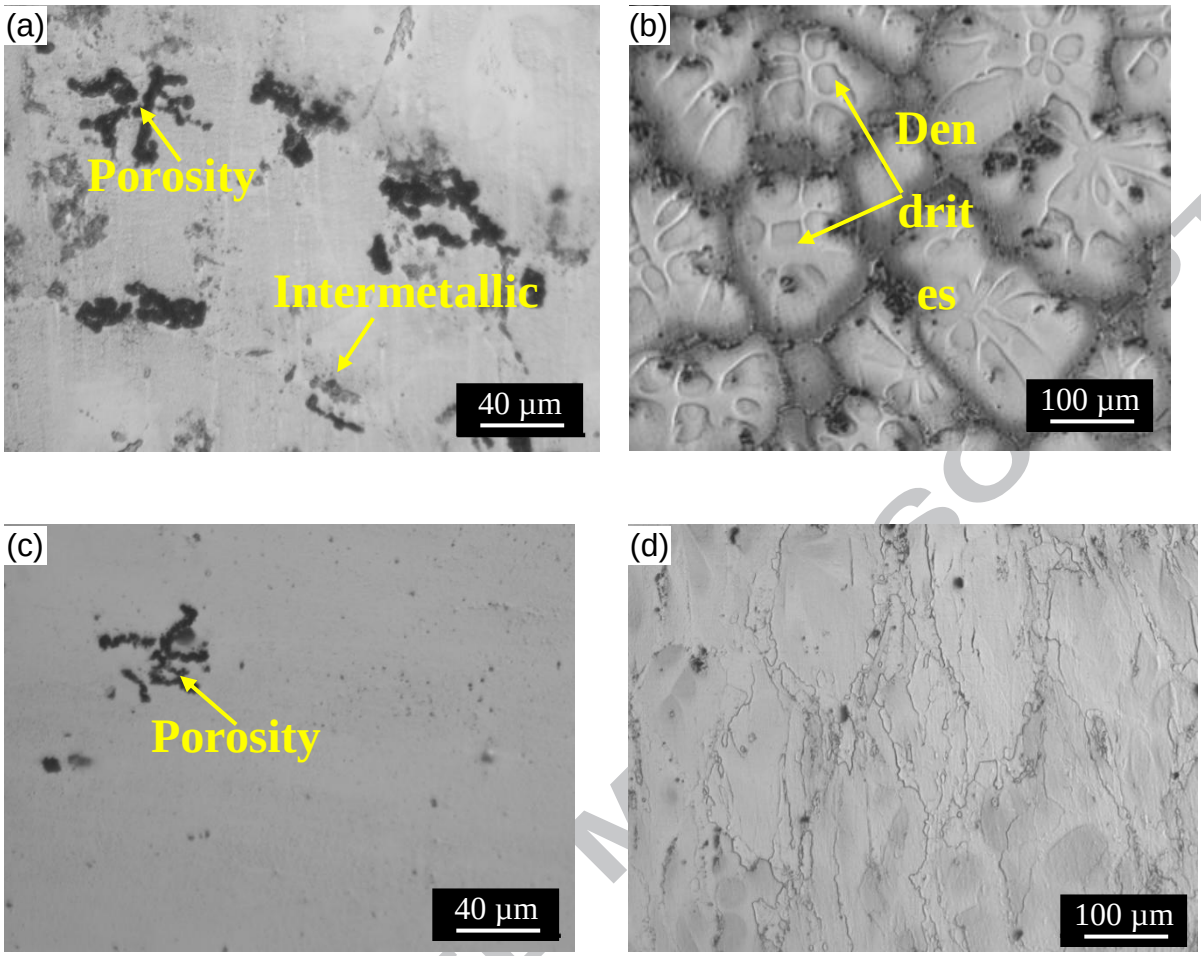

Figure 3 Typical optical microstructures of as-cast ZK60 in unetched (a), and etched conditions (b) and forged ZK60 in unetched (c) and etched conditions (d)

ACCEPTED MANUSCRIPT

ACCEPTED MANUSCRIPT

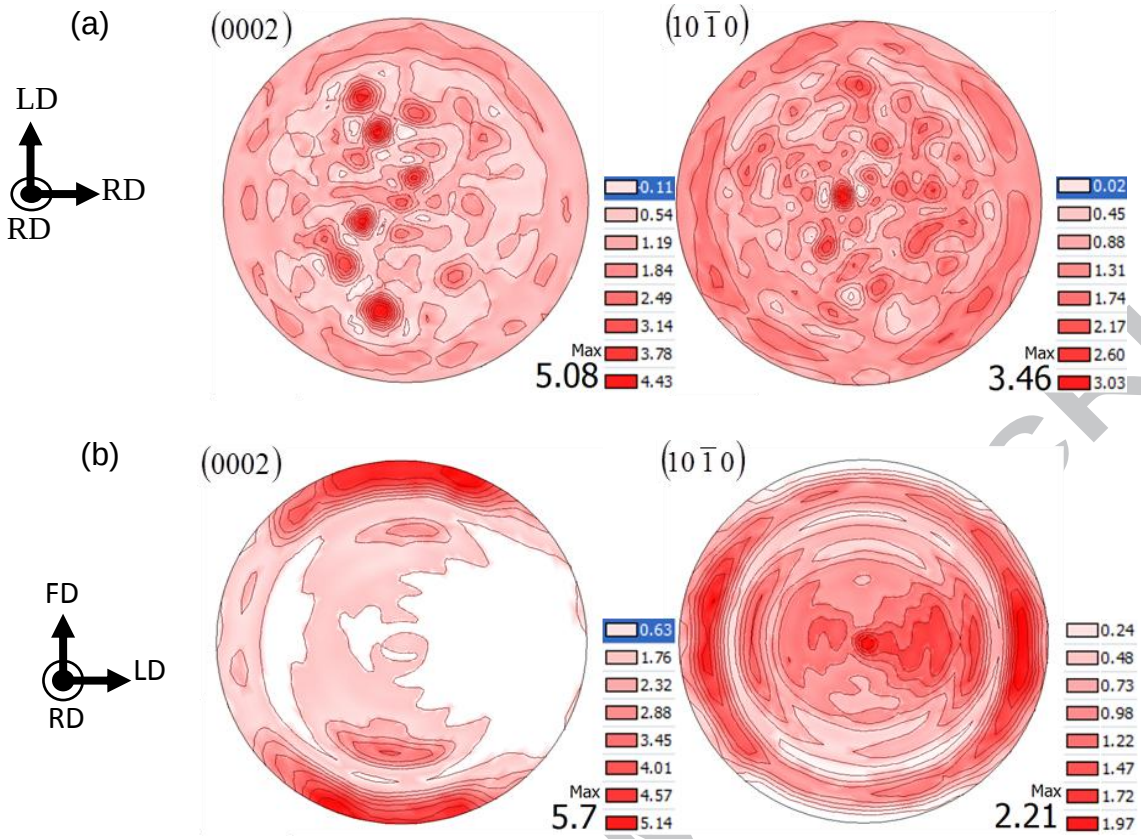

Figure 4. The (0002) basal and $(10\bar{1}0)$ prismatic pole figures (PF) for (a) as-cast ZK60, (b) cast-forged ZK60 Mg alloy [39]

ACCEPTED MANUSCRIPT

ACCEPTED MANUSCRIPT

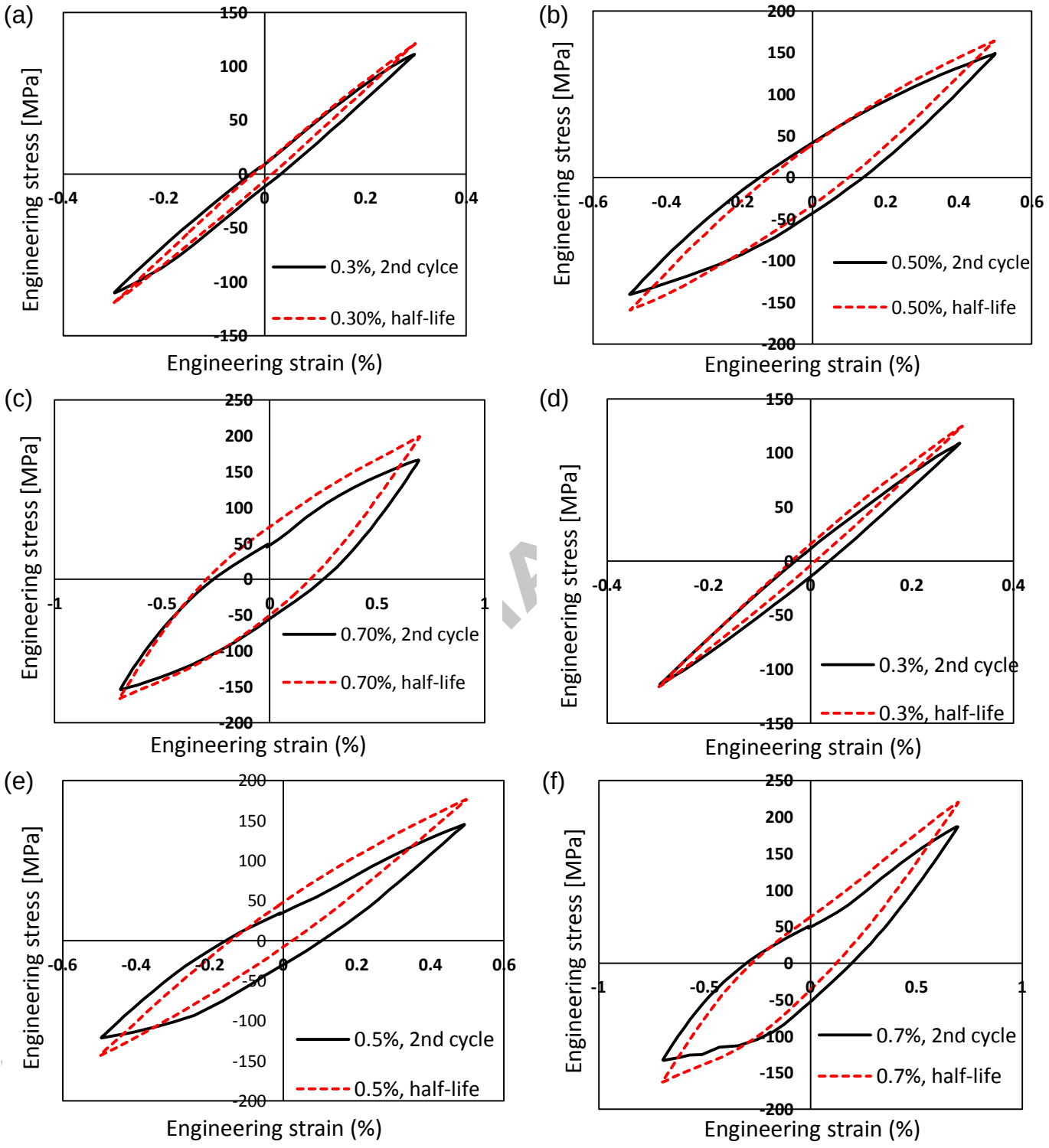

Figure 5. Typical engineering stress-engineering strain hysteresis loops for the as-cast (a, b, c) and forged (d, e, f) ZK60 Mg alloy at different total strain amplitudes of 0.3% (a, d), 0.5% (b, e), and 0.7% (c, f)

ACCEPTED MANUSCRIPT

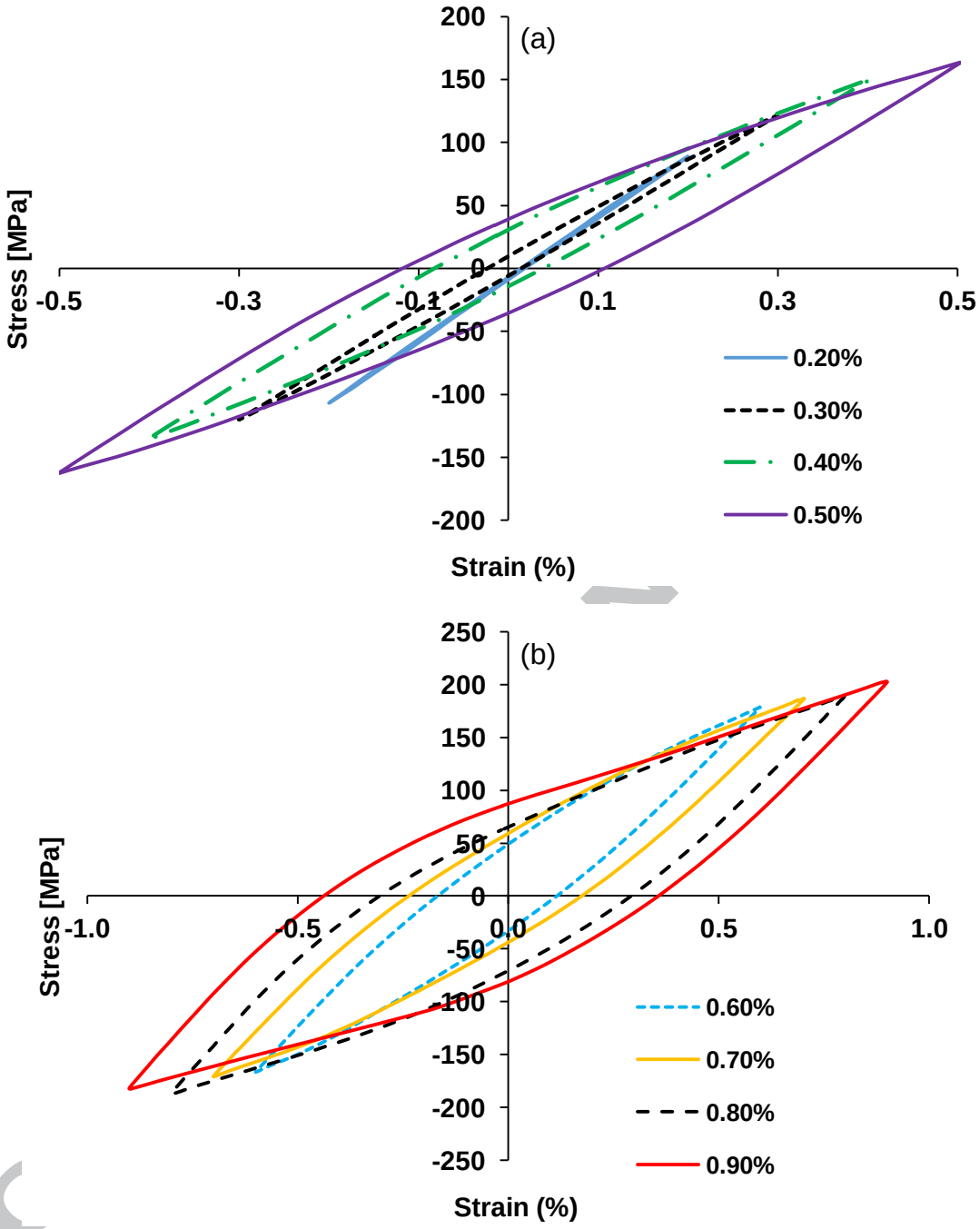

Figure 6. Half-life hysteresis loops for as-cast ZK60 obtained from fully-reversed strain-controlled fatigue tests at different strain amplitudes of (a) 0.2 -0.5% and (b) 0.6-0.9%.

ACCEPTED MANUSCRIPT

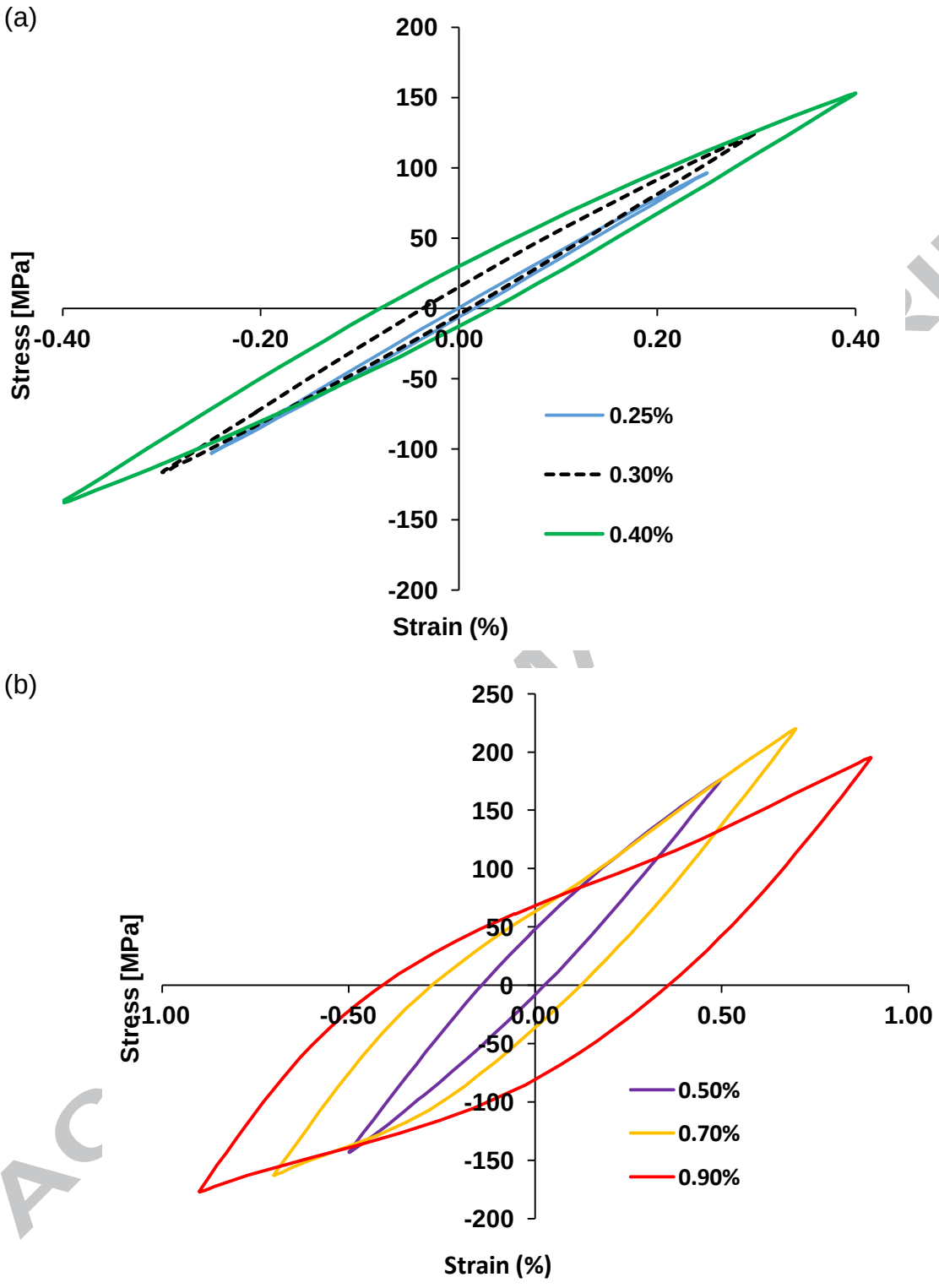

Figure 7. Half-life hysteresis loops for forged ZK60 obtained from fully-reversed strain-controlled fatigue tests at different strain amplitudes of (a) 0.2 -0.4% and (b) 0.5-0.9%.

ACCEPTED MANUSCRIPT

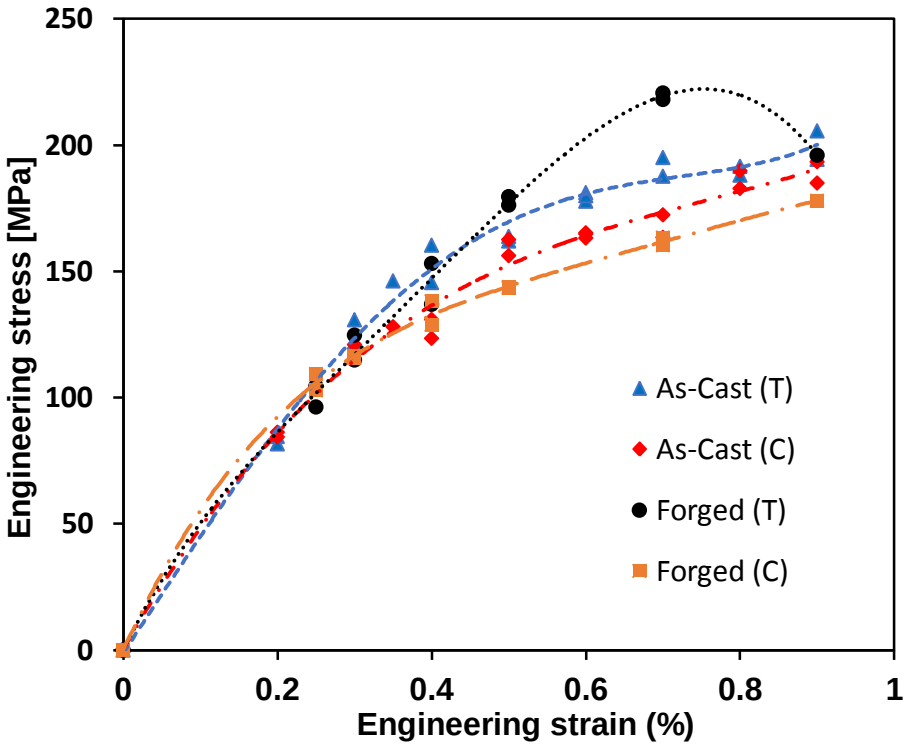

Figure 8. Cyclic behavior of as-cast and forged ZK60 obtained by connecting the peak stresses of the half-life hysteresis loops at different strain amplitudes
Note: T is for tensile peaks on and C is for compressive peaks

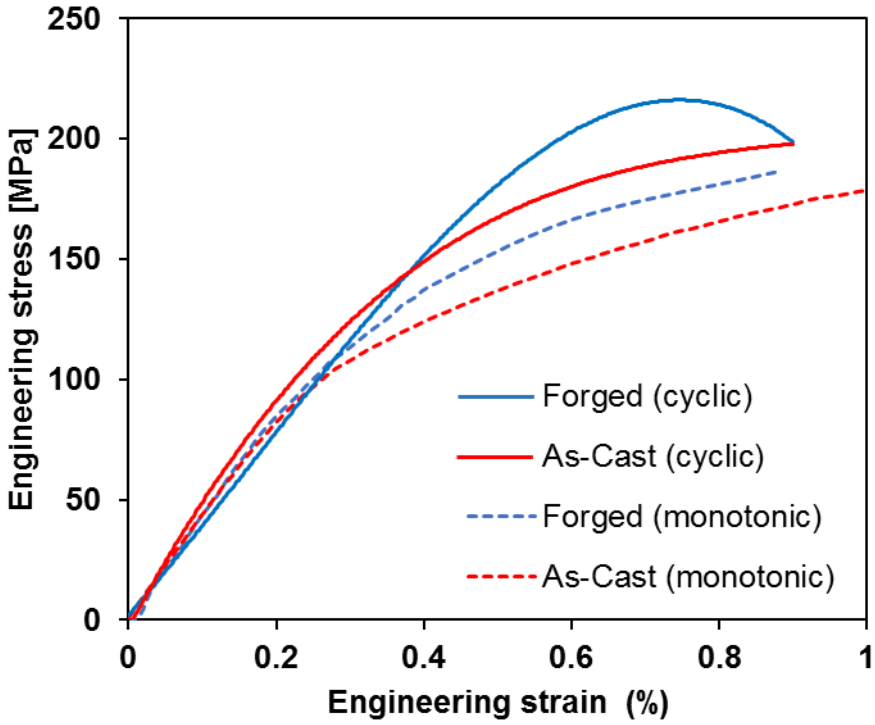

Figure 9. Comparison of the cyclic tensile and quasi-static tensile behavior for as-cast and forged ZK60

ACCEPTED MANUSCRIPT

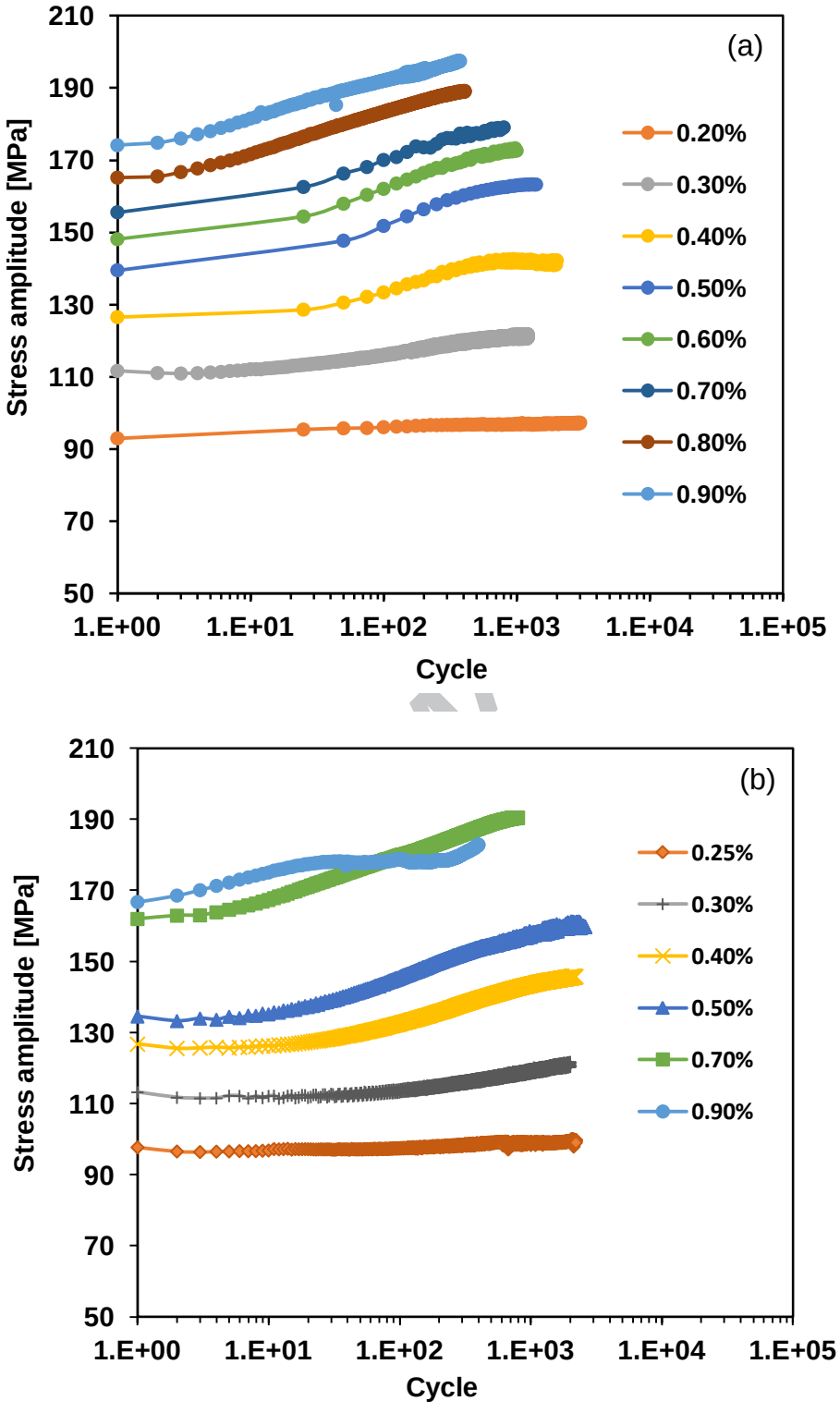

Figure 10. The variation of stress amplitude vs. number of cycles for (a) as-cast and (b) forged ZK60 under different strain amplitudes

ACCEPTED MANUSCRIPT

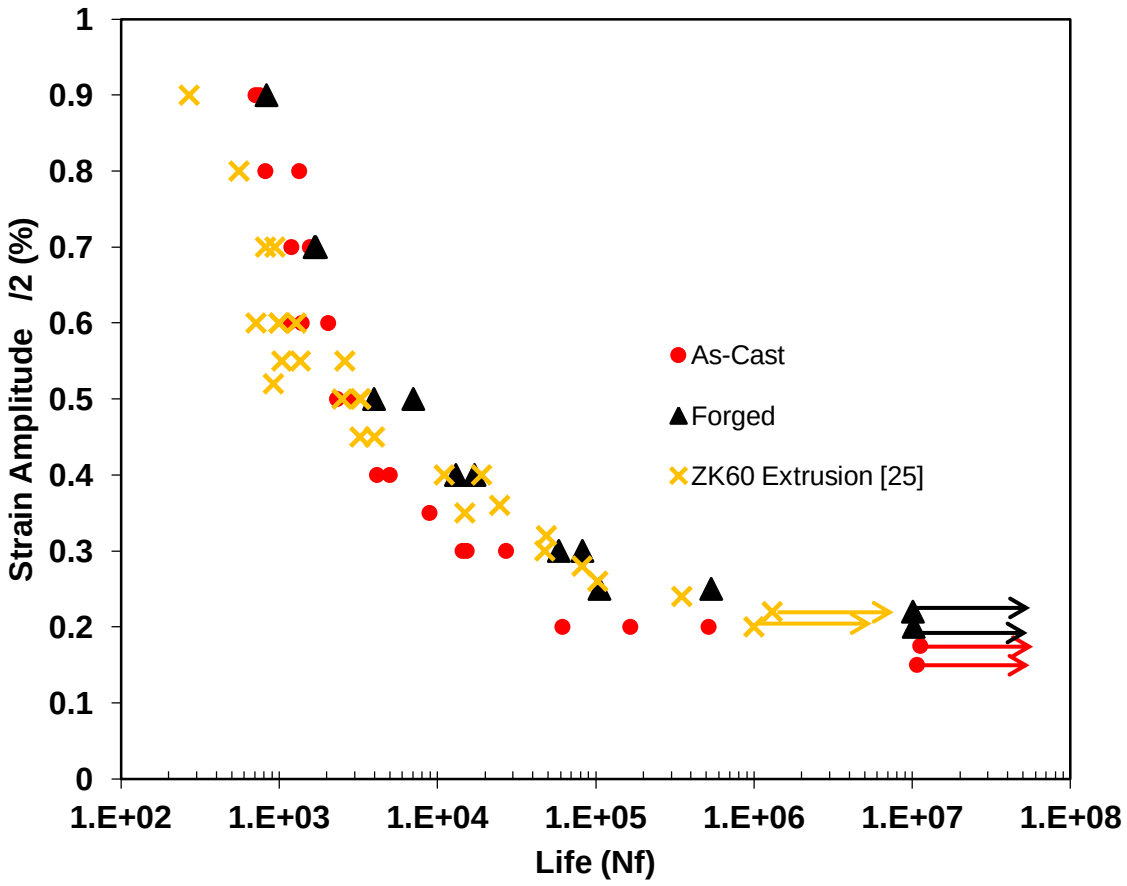

Figure 11. Strain-life data obtained from fully-reversed strain controlled cyclic tests for cast and cast-forged ZK60

ACCEPTED

ACCEPTED MANUSCRIPT

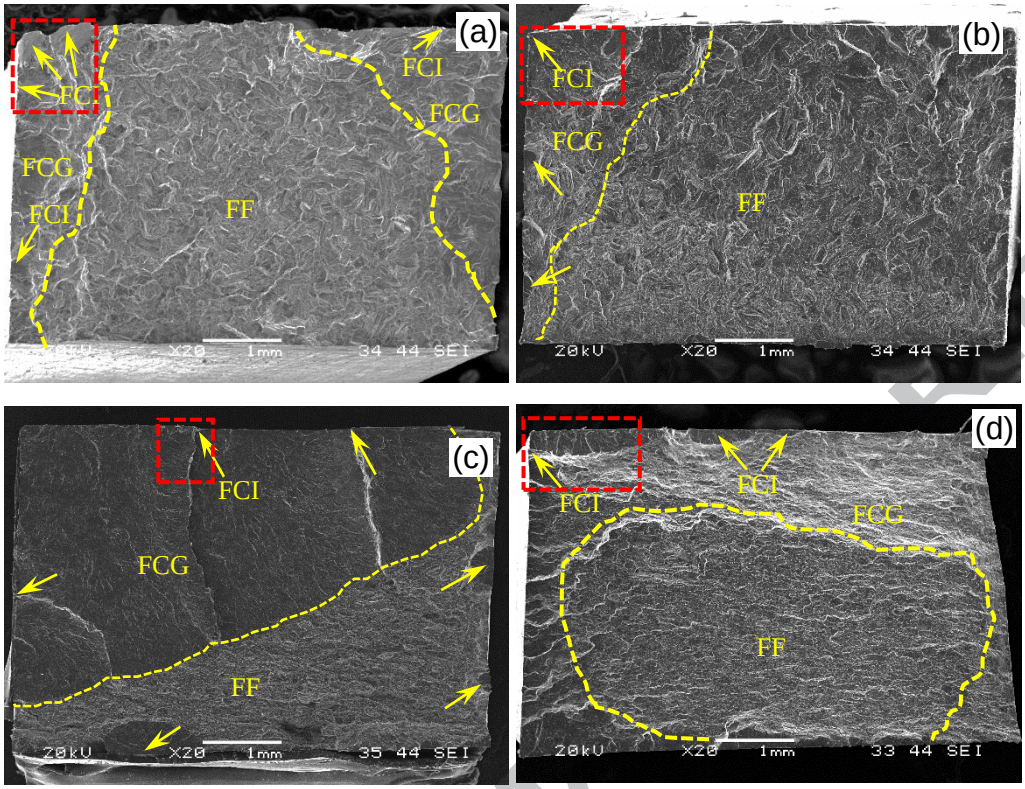

Figure 12. SEM images of fatigue fracture surfaces of ZK60 Mg alloy at different strain amplitudes (a) as-cast at ε_a =0.5%, (b) as-cast at ε_a =0.9%, (c) forged at ε_a =0.5%, and (d) forged at ε_a =0.9% (Yellow arrows indicate the position of FCI sites, and the dashed lines represent the boundary between the FCG and the FF zones)

ACCEPTED MANUSCRIPT

ACCEPTED MANUSCRIPT

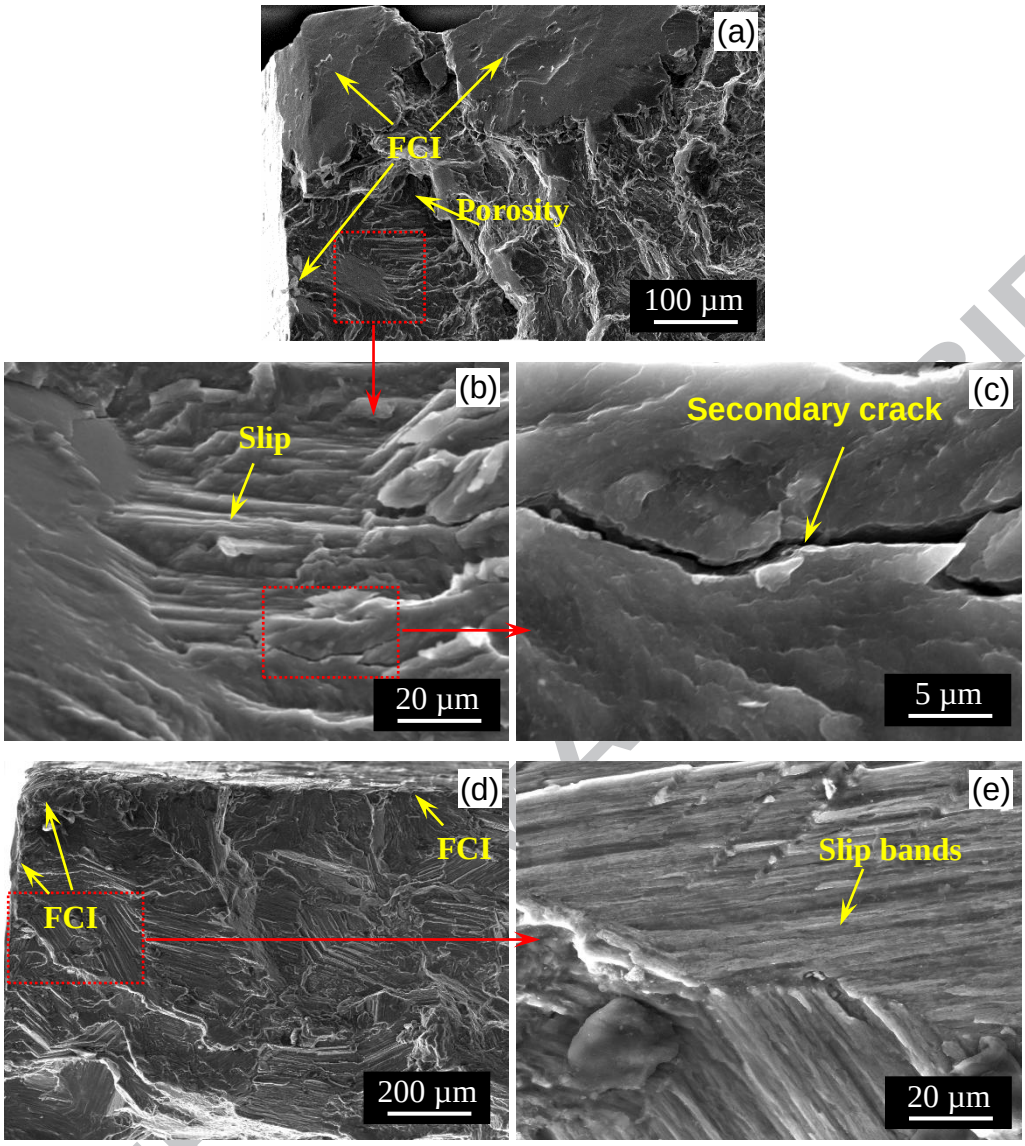

Figure 13. SEM images of FCI locations in as-cast ZK60 tested at strain amplitudes of ε_a =0.5% (a-c), and ε_a =0.9% (d, e)

ACCEPTED MANUSCRIPT

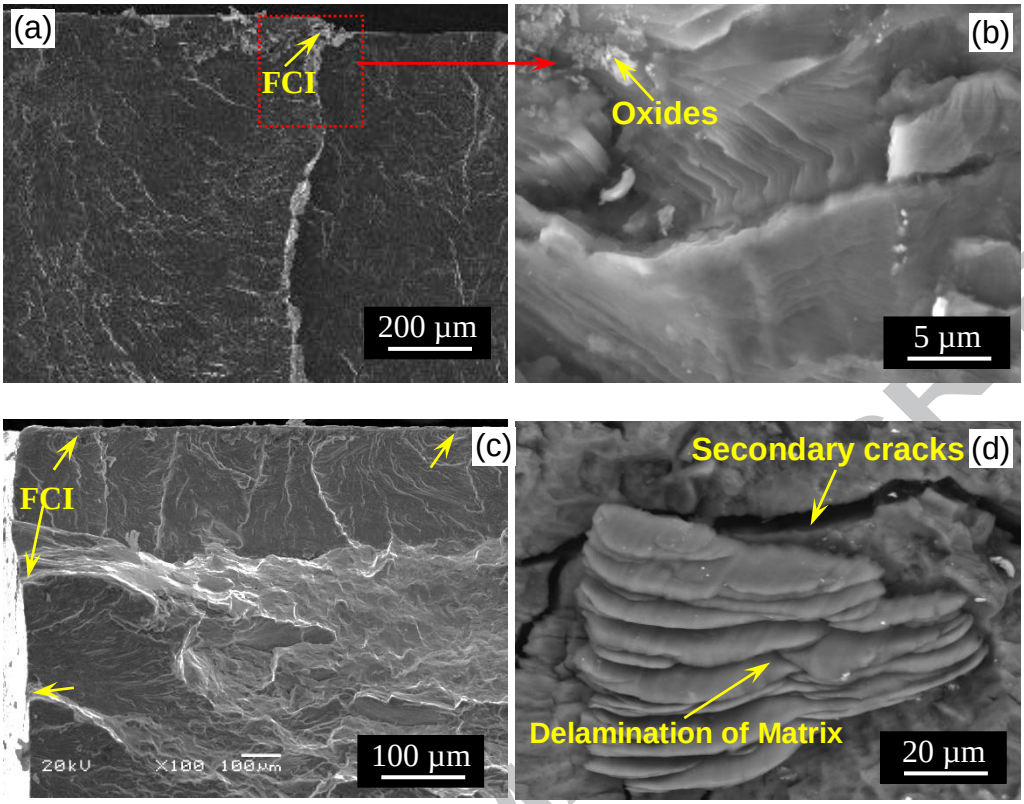

Figure 14. SEM images of fatigue fracture surfaces for cast forged ZK60 tested at a strain amplitude of 0.5% (a, b) and 0.9% (c, d) showing the crack initiation sites with (d) secondary cracks and delamination of the matrix.

ACCEPTED MANUSCRIPT

ACCEPTED MANUSCRIPT

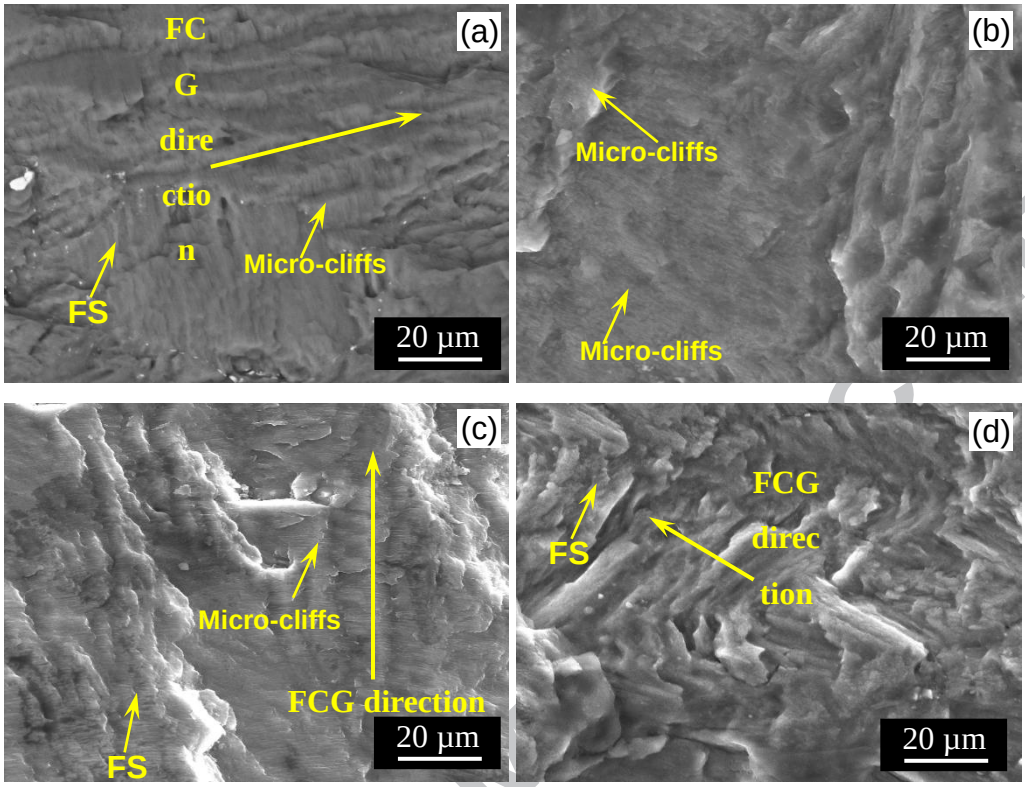

Figure 15. SEM images of the FCG regions of ZK60 under different strain amplitudes (a) as-cast at ε_a =0.5%, (b) as-cast at ε_a =0.9%, (c) forged at ε_a =0.5%, and (d) forged at ε_a =0.9%

ACCEPTED MANUSCRIPT

ACCEPTED MANUSCRIPT

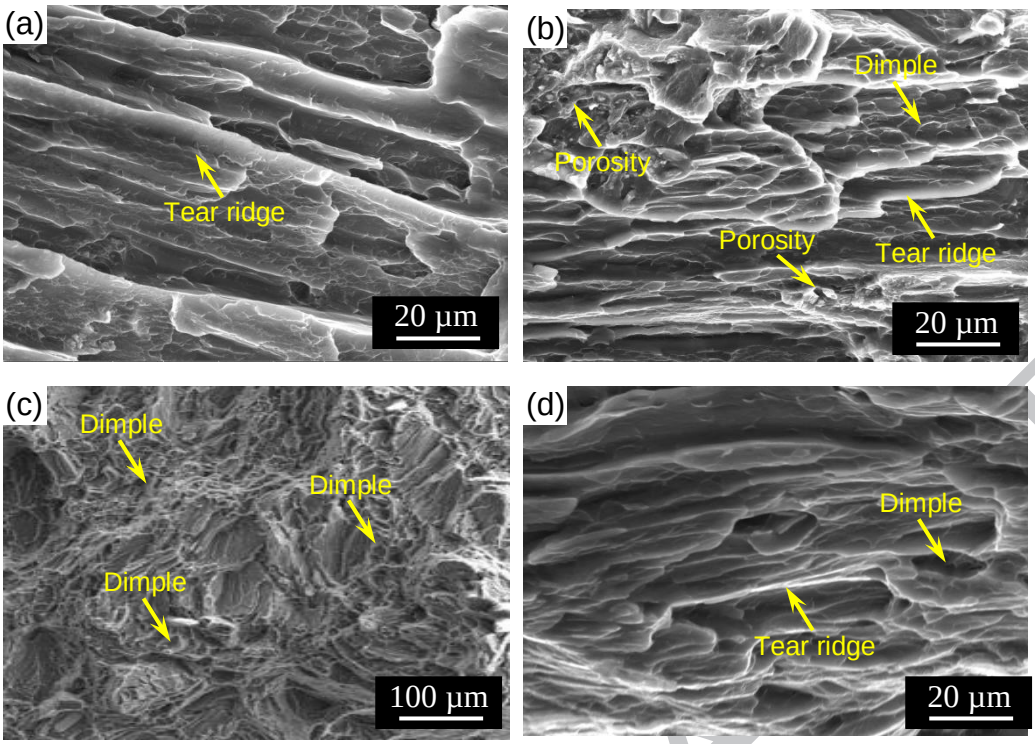

Figure 16. SEM images of the FF regions of ZK60 under different strain amplitudes (a) as-cast at ε_a =0.5%, (b) as-cast at ε_a =0.9%, (c) forged at ε_a =0.5%, and (d) forged at ε_a =0.9%

ACCEPTED MANUSCRIPT

ACCEPTED MANUSCRIPT

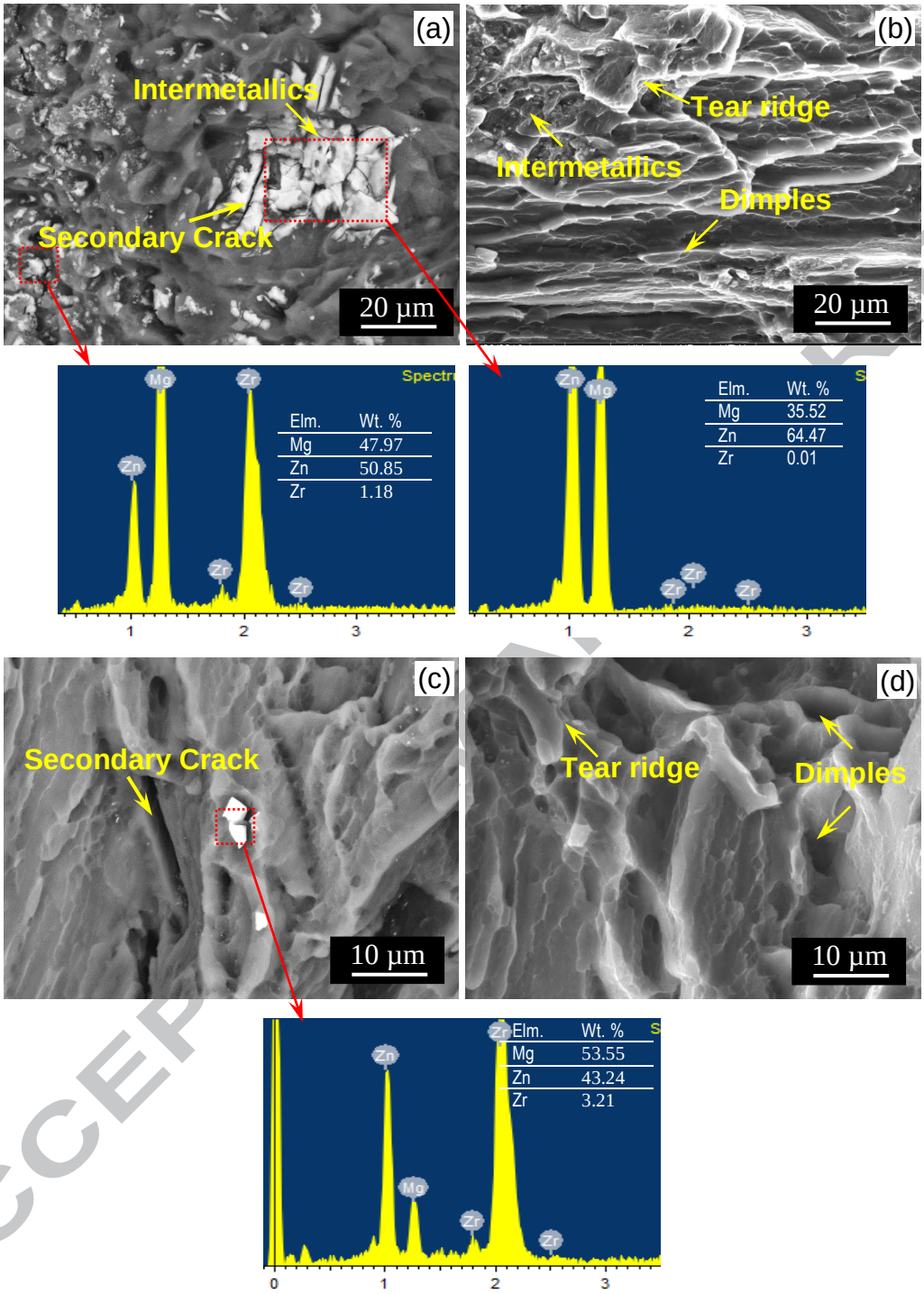

Figure 17. SEM images with EDX spectrums of the FF regions of ZK60 under different strain amplitudes (a) as-cast at ε_a =0.5%, (b) as-cast at ε_a =0.9%, (c) forged at ε_a =0.5%, and (d) forged at ε_a =0.9%

ACCEPTED MANUSCRIPT

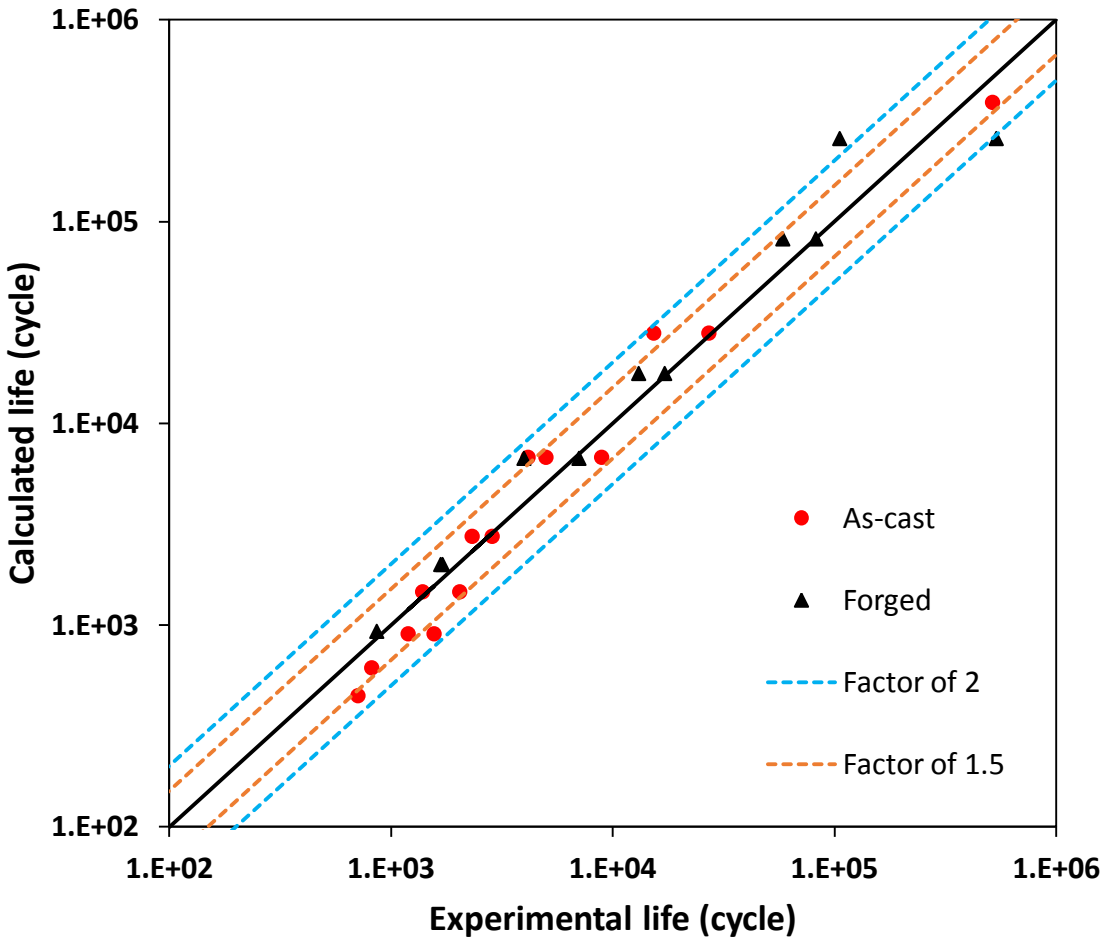

Figure 18. Predicted life vs. experimental life for as-cast and forged ZK60 Mg alloy using the Coffin-Manson model

ACCEPTE

ACCEPTED MANUSCRIPT

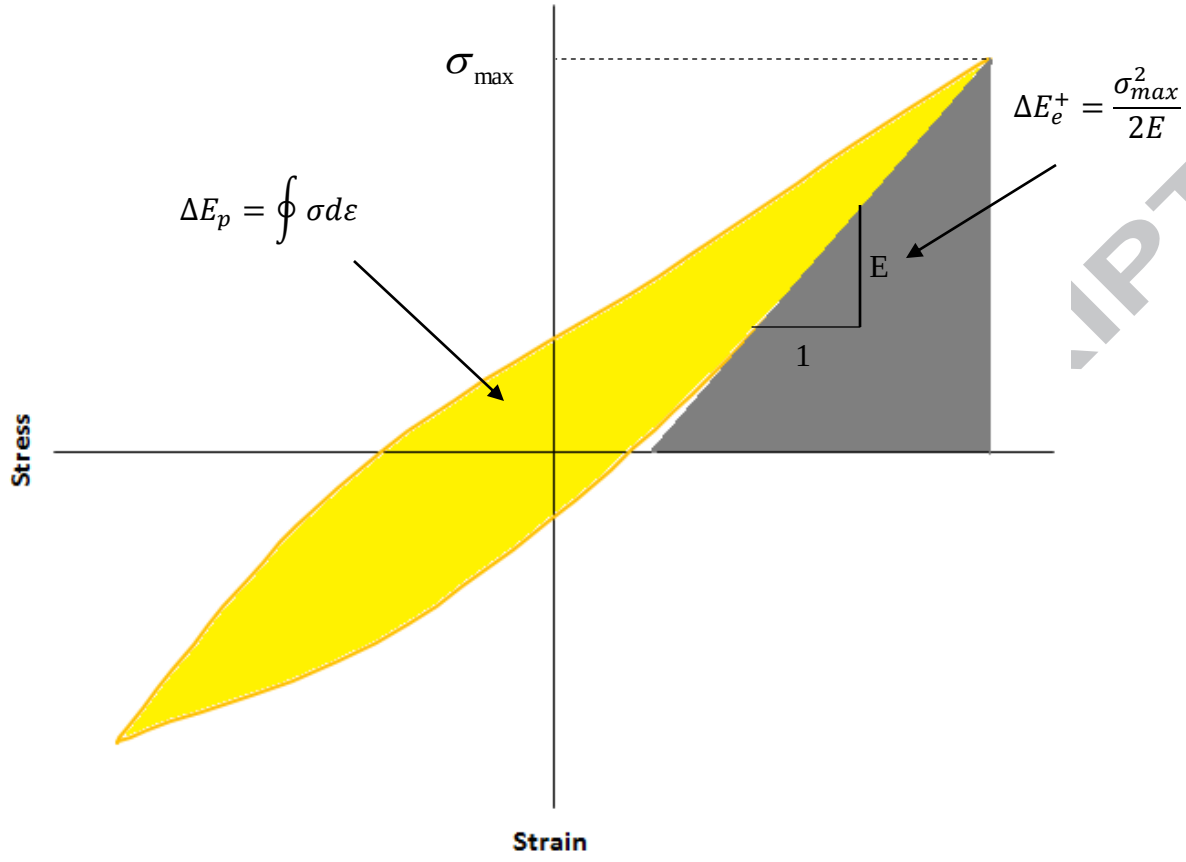

Figure 19. Schematic illustration of positive elastic and plastic strain energy densities [74]

ACCEPTED

ACCEPTED MANUSCRIPT

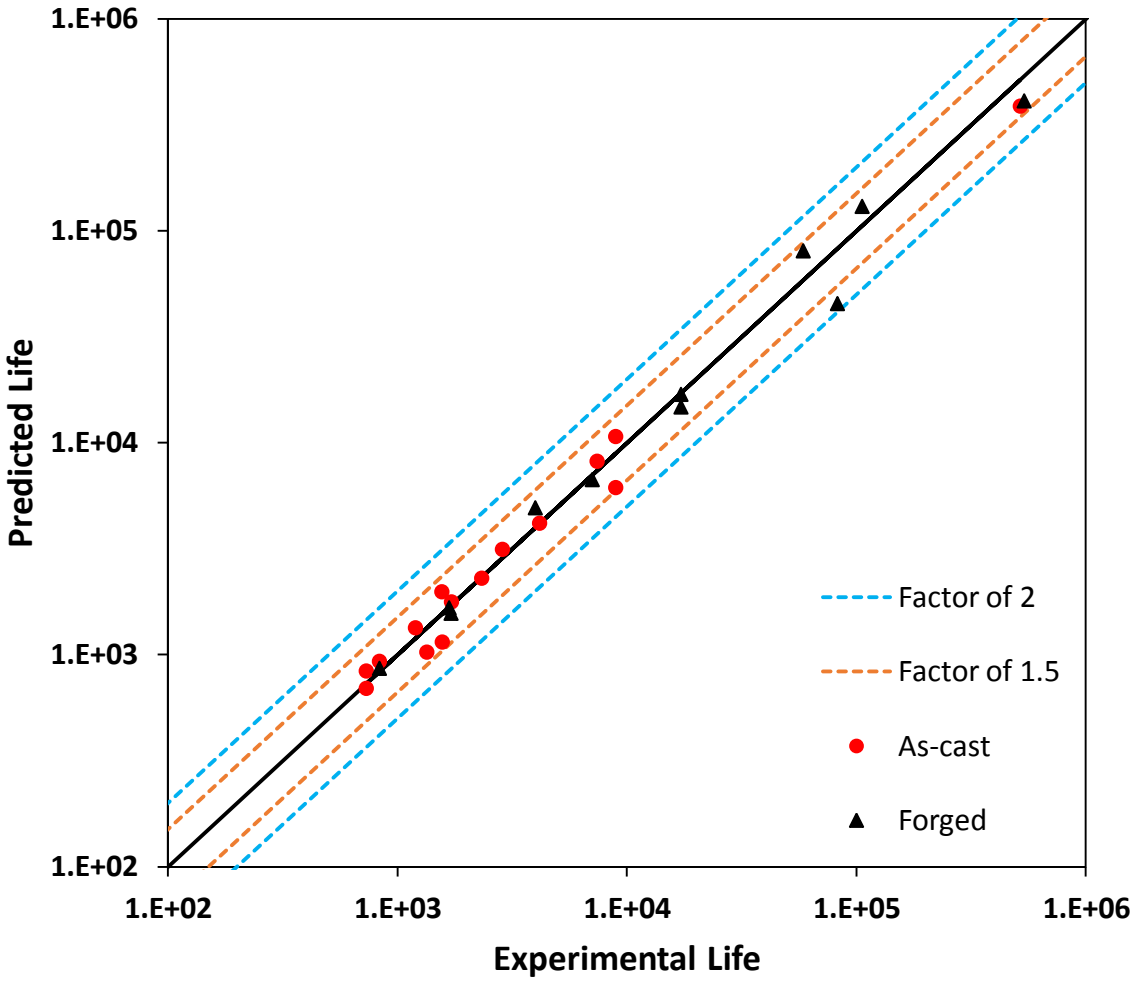

Figure 20. Predicted life versus the experimental life for as-cast and forged ZK60 Mg alloy using the JV fatigue model

ACCEPT

ACCEPTED MANUSCRIPT

Table 2. Mechanical properties of as-cast and forged ZK60 under monotonic tensile loading

	0.2% offset yield strength (MPa)	Ultimate tensile strength (MPa)	Fracture strain (%)
As-Cast	138 ± 0	279 ± 3	15 ± 1
Forged	163 ± 10	286 ± 4	26 ± 3

ACCEPTED MANUSCRIPT

ACCEPTED MANUSCRIPT

Table 3. Cyclic tests summary for the half-life cycle for as-cast and forged ZK60 Mg alloy

Specimen condition	Strain amplitude (%)	Elastic strain amplitude (%)	Plastic strain amplitude (%)	max stress [MPa]	min stress[MPa]	Life	Elastic strain energy density[MJ/m3]	Plastic strain energy density[MJ/m3]
As-cast	0.9	0.439	0.461	198	-197	750	0.44	1.95
	0.9	0.428	0.472	203	-183	709	0.46	1.95
	0.8	0.420	0.380	191	-188	1338	0.40	1.47
	0.8	0.421	0.379	192	-186	818	0.41	1.48
	0.7	0.407	0.293	187	-167	1563	0.39	0.99
	0.7	0.398	0.302	187	-171	1194	0.39	0.99
	0.6	0.391	0.209	185	-167	1388	0.38	0.67
	0.6	0.384	0.216	179	-166	2040	0.36	0.67
	0.5	0.359	0.141	164	-160	2858	0.30	0.49
	0.5	0.363	0.137	164	-163	2321	0.30	0.49
	0.4	0.315	0.085	160	-123	4149	0.28	0.24
	0.4	0.314	0.086	149	-134	4996	0.25	0.23
	0.3	0.271	0.029	122	-121	14417	0.17	0.07
	0.3	0.269	0.031	128	-114	15299	0.18	0.07
	0.3	0.256	0.044	114	-117	27137	0.15	0.06
	0.2	0.184	0.016	81	-84	516579	0.07	0.01
	0.2	0.190	0.010	85	-87	165385	0.08	0.01
	0.175	0.175	0.000	73	-74	>10000001	0.06	0.00
	0.15	0.150	0.000	66	-64	>10000000	0.05	0.00
Forged	0.9	0.416	0.484	197	-179	832	0.43	1.81
	0.7	0.420	0.280	220	-161	1707	0.54	1.01
	0.7	0.427	0.273	221	-164	1674	0.54	0.99
	0.5	0.359	0.141	180	-144	3976	0.36	0.37
	0.5	0.355	0.145	176	-143	7041	0.34	0.38
	0.4	0.324	0.076	154	-139	13090	0.26	0.28
	0.4	0.295	0.105	138	-130	17152	0.21	0.28
	0.3	0.256	0.044	125	-116	58490	0.17	0.11
	0.3	0.268	0.032	115	-117	82445	0.15	0.11
	0.25	0.238	0.012	105	-110	105616	0.12	0.03
	0.25	0.221	0.029	97	-104	536971	0.10	0.03
	0.22	0.220	0.000	92	-93	>10000000	0.09	0.00
	0.2	0.200	0.000	88	-88	>10000000	0.09	0.00

ACCEPTED MANUSCRIPT

ACCEPTED MANUSCRIPT

Table 4. Coffin-Manson parameters for the as-cast and cast-forged ZK60 magnesium alloy

fatigue parameter	As-cast ZK60	Forged ZK60
σ_f' (MPa)	442	510
b	-0.12	-0.12
ε_f'	0.31	0.37
c	-0.62	-0.59

ACCEPTED MANUSCRIPT

ACCEPTED MANUSCRIPT

Table 5. The energy parameters of JV fatigue model for the tested as-cast and cast-forged ZK60 magnesium alloy

fatigue parameter	As-cast ZK60	Forged ZK60
E_e' (MJ/m^3)	4.20	4.30
B	-0.30	-0.27
E_f' (MJ/m^3)	1525.50	290.60
C	-0.92	-0.70

ACCEPTED MANUSCRIPT

ACCEPTED MANUSCRIPT

Highlights

- Cyclic behavior of ZK60 Mg alloy cast prior to and after forging process is studied.
- Microstructure modification after forging leads to better fatigue response.
- Forged alloy asymmetric fatigue behavior is due to the induced sharp basal texture.
- $ZnZr_2$ and $MgZn_2$ intermetallics are main source of crack initiation.
- An energy-based fatigue life model closely estimated the cyclic life.

ACCEPTED MANUSCRIPT